Integrated Ocean Drilling Program Expedition 315 Preliminary Report

NanTroSEIZE Stage 1A: NanTroSEIZE Megasplay Riser Pilot

16 November–18 December 2007

Juichiro Ashi, Siegfried Lallemant, Hideki Masago, and the Expedition 315 Scientists

Publisher's notes

Disclaimer

February 2008

Expedition 315 participants

Expedition 315 scientists

Juichiro Ashi
Co-Chief Scientist
Ocean Research Institute
The University of Tokyo
1-15-1 Minamidai, Nakano-ku
Tokyo 164-8639
Japan
ashi@ori.u-tokyo.ac.jp

Siegfried Lallemant
Co-Chief Scientist
Département des Sciences de la Terre et de
    l'Environnement
Université de Cergy-Pontoise
5 mail, Gay-Lussac, Neuville-sur-Oise
95031 Cergy-Pontoise Cedex
France
siegfried.lallemant@u-cergy.fr

Hideki Masago
Expedition Project Manager
Center for Deep Earth Exploration
Japan Agency for Marine-Earth Science and
    Technology
3173-25 Showa-machi, Kanazawa-ku
Yokohama, Kanagawa 236-0001
Japan
masagoh@jamstec.go.jp

Jan H. Behrmann
Structural Geology
Leibniz Institute of Marine Sciences
IFM-GEOMAR
Wischhofstrasse 1-3
24148 Kiel
Germany
jbehrmann@ifm-geomar.de

Babette Boeckel
Micropaleontology
Department of Geosciences
Bremen University
Klagenfurterstrasse
28359 Bremen
Germany
bboeckel@uni-bremen.de

Timothy Byrne
Structural Geology
Center for Integrative Geosciences
University of Connecticut
U-2045, 354 Mansfield Road
Storrs CT 06269
USA
tim.byrne@uconn.edu

Gerome Calves
Sedimentology
Department of Geology and Petroleum
    Geology
University of Aberdeen
Meston Building, Kings College
Aberdeen AB24 3UE
United Kingdom
g.calves@abdn.ac.uk

Vincent Famin
Structural Geology
LSTUR-IPGP
Universite de la Reunion
15, Avenue Rene Cassin, BP7151
97715 Saint Denis messag Cedex 9
France
yfamin@univ-reunion.fr

Junhua Guo
Sedimentology
Department of Geological Sciences
University of Missouri
101 Geology Building
Columbia MO 65211
USA
jg2kc@mizzou.edu

Yoshitaka Hashimoto
Sedimentology
Department of Natural Environmental Science
Faculty of Science, Kochi University
Akebonocyo 2-5-1
Kochi 780-8520
Japan
hassy@cc.kochi-u.ac.jp

Hiroki Hayashi
Micropaleontology
Department of Geoscience
Interdisciplinary Faculty of Science
    and Engineering
Shimane University
1060 Nishikawatsucho, Matsue
Shimane 690-8504
Japan
hayashi@riko.shimane-u.ac.jp

Pierre Henry
Physical Properties
CNRS, CEREGE—College de France
Europole de l'Arbois BP80
13545 Aix en Provence Cedex 04
France
henry@cdf.u-3mrs.fr

Tetsuro Hirono
Physical Properties
Department of Earth and Space Science
Graduate School of Science
Osaka University
1-1 Machikaneyama-cho, Toyonaka-shi
Osaka 560-0043
Japan
hirono@ess.sci.osaka-u.ac.jp

Samuel M. Hulme
Inorganic Geochemistry
Hawaii Institute of Geophysics
    and Planetology (HIGP)
1680 East-West Road, POST 504
Honolulu HI 96822
USA
hulme@higp.hawaii.edu

Anna Henriikka Kaksonen
Microbiology
Department of Chemistry and Bioengineering
Tampere University of Technology
PO Box 541
FIN-33101 Tampere
Finland
anna.kaksonen@tut.fi

Kyuichi Kanagawa
Structural Geology
Department of Earth Sciences
Chiba University
1-33 Yayoi-cho, Inage-ku
Chiba 263-8522
Japan
kyu_kanagawa@faculty.chiba-u.jp

Toshiya Kanamatsu (Specialty Coordinator)
Paleomagnetism
IFREE, Japan Agency for Marine-Earth Science
    and Technology
2-15 Natushima-cho
Yokosuka, Kanagawa 237-0061
Japan
toshiyak@jamstec.go.jp

Achim Kopf
Physical Properties
Department of Geosciences
Bremen University
Leobener Strasse, MARUM Building
28359 Bremen
Germany
akopf@uni-bremen.de

Jonathan C. Lewis
Structural Geology
Department of Geoscience
Indiana University of Pennsylvania
114 Walsh Hall
Indiana PA 15705
USA
jclewis@iup.edu

William John Likos
Physical Properties
Department of Civil and Environmental
    Engineering
University of Missouri
Lafferre Hall
Columbia MO 65211
USA
likosw@missouri.edu

Josep Maria Pares
Paleomagnetism
Department of Geological Sciences
University of Michigan
2534 CCL Building
Ann Arbor MI 48109
USA
jmpares@umich.edu

Hiroyuki Saito
Organic Geochemistry
Department of Natural History Science
Hokkaido University
N10 W8, Kita-ku
Sapporo 060-0810
Japan
hsaito@mail.sci.hokudai.ac.jp

Friederike Schmidt-Schierhorn
Physical Properties/Heat Flow
FB Geowissenschaften
Universität Bremen
Postfach 330 440
28334 Bremen
Germany
fss@uni-bremen.de

Hitoshi Tomaru
Inorganic Geochemistry
New Energy Resources Research Center
Kitami Institute of Technology
165 Koen-cho, Kitami
Hokkaido 090-8507
Japan
tomaru@mail.kitami-it.ac.jp

Michael Underwood
  (Specialty Coordinator)
Sedimentology
Department of Geological Sciences
University of Missouri
101 Geology Building
Columbia MO 65211
USA
underwoodm@missouri.edu

Wen-Lu Zhu
Physical Properties
Department of Geology and Geophysics
Woods Hole Oceanographic Institute
360 Woods Hole Road, MSC 25
Woods Hole MA 02543-1541
USA
wzhu@whoi.edu

NanTroSEIZE specialty coordinator

Geoff Wheat (16–28 November 2007)
Geochemistry
School of Fisheries and Ocean Sciences
University of Alaska Fairbanks
PO Box 475
Moss Landing CA 99775
USA
wheat@mbari.edu

Shipboard personnel and technical representatives

Captains (Seadrill)
Kazuo Ichiyama
Yuji Onda

Offshore Installation Managers (Seadrill)
Simon Cook
Scott Pederson

Operations Superintendents (CDEX)
Tsuyoshi Abe
Ikuo Sawada

Coring Supervisor (AAI)
James T. Aumann

Curators (Marine Works Japan)
Yohei Arakawa
Satoshi Hirano

Downhole Tools Engineers
Dean Ferrell (USIO)
Yoshinori Sanada (CDEX)

Drilling Engineers (CDEX)
Kazutaka Higuchi
Daiji Ikenomoto
Kunihiro Muta
Tomokazu Saruhashi

Information Technology Manager (CDEX)
Kyoma Takahashi

Laboratory Officers (Marine Works Japan)
Kazuhiro Hayashi
Toshikatsu Kuramoto

**Assistant Laboratory Officers
  (Marine Works Japan)**
Hiroaki Muraki
Tomoyuki Tanaka

**Laboratory Technicians
  (Marine Works Japan)**
Akihiko Fujihara
Shoko Fujii
Toru Fujiki
Yuji Fuwa
Yasushi Hashimoto
Yuya Hitomi
Tetsuharu Iino
Masumi Ishimori
Yusuke Kawana
Yoshiki Kido
Yuji Kotani

Ryo Kurihara
Lena Maeda
Shunsuke Miyabe
Jyunnichi Mizuno
Takami Mori
Sohichi Moriya
Masahiro Nishimura
Takuroh Noguchi
Yoshifumi Noiri
Yuko Sagawa
Masumi Sakaguchi
Yusuke Sato
Kentaro Shiraishi
Akira So
Kazuhiro Sugiyama
Kei Suminaga
Nami Suzuki
Takahiro Suzuki
Tamami Ueno

Publication Assistants (USIO)
Virginia Lowe
Debbie Partain

Technical Adviser (CDEX)
Kazumasa Kato

Wellsite Geologists (CDEX)
Chikara Hiramatsu
Gyuhwan Jo
Toshio Kaminishi
Arata Kato
Kiyoshi Koide
Fujio Yamamoto

Abstract

During Integrated Ocean Drilling Program Expedition 315, coring at two planned riser drilling sites was conducted. For Nankai Trough Seismogenic Zone Experiment (NanTroSEIZE) Stage 2, 3.5 km riser drilling is planned at Site C0001. We cored at this site to 458 m core depth below seafloor (CSF; IODP Method A: core expansion lengths overlap [are not scaled]) and cut 59 cores (31 with the hydraulic piston coring system [HPCS], 2 with the extended shoe coring system [ESCS], and 26 with the rotary core barrel [RCB]) from five holes covering a slope basin (Unit I) and the top 250 m of the underlying accretionary prism (Unit II). The slope basin is composed mainly of Quaternary to late Pliocene silty clay and clayey silt with intercalations of volcanic ash. The boundary between Units I and II, identified at 207.17 m CSF, is an unconformity characterized by a thick sand layer. Unit II is composed of more consolidated mud-dominated sediments of late Pliocene to late Miocene age. Structural style and stress state vary widely across a highly deformed zone at 220 m CSF. A normal fault indicating northeast–southeast extension is dominant above this zone; however, a few thrust faults dipping at 50° were encountered just above the deformed zone. These thrust faults are consistent with the northwest–southeast shortening subparallel to the direction of plate convergence. On the other hand, many thrust and strike-slip faults as well as a normal fault are found below the 220 m CSF deformed zone. The geometry and kinematics of planar structures display great variation. Fault plane solutions computed from normal and thrust faults are consistent with northeast–southwest extension and northwest–southeast shortening, respectively. A total of 48 whole-round samples were taken for interstitial geochemistry. Obtained data show meaningful trends for most elements, and potential contamination of drilling fluid is taken into consideration; however, changing trends do not necessarily correspond to unit boundaries. Methane and ethane concentrations and their ratio (C_1/C_2) decrease with depth to 100 m CSF and remain constant to the base of Unit I. The increase of methane concentrations and C_1/C_2 ratios in Unit II indicate the contribution of biogenic methane. Total organic carbon and calcium carbonate decrease monotonously to the base of Unit I and remain low throughout Unit II. Physical properties also show a clear break at the boundary between Units I and II. Porosity decreases downhole within each unit; however, there is a gap across the unit boundary. Thermal conductivity is almost constant throughout Unit I and decreases with depth in Unit II. Downhole temperature was measured with the advanced piston corer temperature tool (APCT3) at seven depths to 170.98 m CSF and yielded a generally linear downhole temperature increase, with a gradient of 0.042°C/m.

For NanTroSEIZE Stage 3, 6 km riser drilling is planned at Site C0002. We drilled to 1057 m CSF, cored the intervals from seafloor to 204 m CSF and 475 to 1057 m CSF, and cut 86 cores (18 with the HPCS, 2 with the ESCS, and 66 with the RCB) from three holes. We penetrated the basal unconformity of the Kumano forearc basin at ~936 m CSF and cored another 120 m into the accretionary prism. The forearc basin sequence was divided into two units based on lithofacies; these units corresponded to Units II and III defined by LWD, respectively. Both units are dominated by mud and mudstone; however, the Unit I contains more sand and silt intercalation and has a much faster sedimentation rate. The age ranges from Quaternary to late Miocene. Underlying accretionary prism materials contain more lithified and deformed sediments. Only one nannofossil event, of late Miocene age, was determined for Unit IV; hence, no significant gap was detected across the unconformity. Faults and shear zones are clustered at certain depths around 700, 920–950, and 1000–1050 m CSF. Three deformation phases were recognized by fault analyses. The earliest phase is a thrust fault (and possibly a strike-slip fault) and exhibits northwest–southeast shortening. Two phases of normal faulting occurred subsequent to thrusting. The first is recorded in shear zones and indicates northeast–southwest extension. The second is recorded in normal faults and indicates north–south extension, consistent with the present stress direction acquired from LWD results. A total of 31 whole-round samples were taken for interstitial water analyses. Changes in concentration for most elements seem to be controlled by unit boundaries. A downward increase of ethane and concomitant decrease of C_1/C_2 ratios in Unit IV suggest some contribution of thermogenic hydrocarbons. Physical properties show complex trends with depth. Downhole temperature was measured at eight depths to 159.0 m CSF and showed an almost linear downhole increase with a gradient of 0.043°C/m, identical to that found at Site C0001.

Introduction

Subduction zones like the Nankai Trough, a region of strong earthquakes (M 8), are especially favorable for study because the entire width (dip extent) of the seismogenic zone ruptures in each great event, so that future rupture areas are perhaps more predictable than for smaller earthquakes. The Nankai Trough region is among the best-studied subduction zones in the world. It has a 1300 y historical record of recurring, and typically tsunamigenic, great earthquakes, including the 1944 Tonankai M 8.2 and 1946 Nankaido M 8.3 earthquakes (Ando, 1975; Hori et al., 2004). The rupture area and zone of tsunami generation for the 1944 event are now reasonably well understood (Ichinose et al., 2003; Baba and Cummins, 2005). Land-based geodetic studies suggest that the plate boundary thrust here is strongly locked (Miyazaki and Heki, 2001). Similarly, the relatively low level of microseismicity near the updip limits of the 1940s earthquakes (Obana et al., 2004) implies significant interseismic strain accumulation on the megathrust; however, recent observations of very low frequency earthquake event swarms apparently taking place within the accretionary prism in the drilling area (Obara and Ito, 2005) demonstrate that interseismic strain is not confined to slow elastic strain accumulation.

Background

Geological setting

The Nankai Trough is a plate convergent margin where the Philippine Sea plate subducts to the northwest beneath the Eurasian plate at a rate of ~4 km/m.y. (Seno et al., 1993). The convergence direction is approximately normal to the trench, and Shikoku Basin sediments are actively accreting at the deformation front (Fig. F1). The Nankai Trough is among the most extensively studied subduction zones in the world, and great earthquakes during the past 3000 y are well documented in historical and archeological records (e.g., Ando, 1975). The Nankai Trough has been selected as a focus site for studies of seismogenesis by both the Integrated Ocean Drilling Program (IODP) and the U.S. MARGINS initiative because of the wealth of geological and geophysical data available, the long historical record of great (M > 8.0) earthquakes, and the direct societal relevance of understanding the generation and impact of tsunamis and earthquakes on the heavily populated coastal region.

The region offshore the Kii Peninsula has been identified as the best location for seis-mogenic zone drilling for several reasons. First, the rupture area of the most recent great earthquake, the 1944 M 8.1 Tonankai event, is well constrained by recent seis-mic and tsunami waveform inversions (e.g., Tanioka and Satake, 2001; Ichinose et al., 2003; Kikuchi et al., 2003). A horizon of significant coseismic slip is reachable by drill-ing with the D/V *Chikyu*. Second, the region offshore the Kii Peninsula is generally typical of the Nankai margin in terms of heat flow and sediment on the incoming plate, in contrast to the area offshore Cape Muroto where previous Deep Sea Drilling Program and Ocean Drilling Program (ODP) drilling has focused and where local stra-tigraphy associated with both basement topography and anomalously high heat flow has been documented (Moore et al., 2001). Third, ocean bottom seismometer cam-paigns and on-land high-resolution geodetic studies (though of short duration) indi-cate significant interseismic strain accumulation (e.g., Miyazaki and Heki, 2001; Obana et al., 2004).

A large out-of-sequence thrust branches from the master décollement ~50 km land-ward of the trench along the drilling transect and forms the trenchward boundary of the Kumano Basin (Figs. F2, F3). Swath-bathymetric and multichannel seismic data show a pronounced, continuous outer ridge of topography extending >120 km along strike, which may be related to the splay fault slip. Remotely operated vehicle (ROV) and submersible surveys along this feature have revealed very steep slopes on either side of the ridge, suggesting recent activity (Ashi et al., 2002, unpubl. data). This fault has been termed a "megasplay" and differs markedly from other out-of-sequence thrusts in several respects:

- The megasplay is continuous along strike, is associated with a significant break in the seafloor slope, and is a strong seismic reflector, suggesting that it is a first-order structural element of the margin.

- Significant long-term slip is documented by sequence boundaries and progressive landward tilting of strata in the Kumano Basin is observed in seismic reflection data.

- The megasplay separates rocks with significantly higher seismic velocity on its landward side from rocks of lower seismic velocity toward the trench, suggesting that it represents a major mechanical discontinuity (Nakanishi et al., 2002).

- The megasplay is geographically coincident with the updip termination of slip dur-ing the 1944 M 8.1 Tonankai event, as inferred from tsunami (Tanioka and Satake, 2001) and seismic (Kikuchi et al., 2003) waveform inversions, and recent structural studies indicate that it may have experienced coseismic slip (e.g., Park et al., 2002).

Mechanical arguments further suggest that the megasplay is the primary coseismic plate boundary near the updip terminus of slip (e.g., Kame et al., 2003; Wang and Hu, 2006).

Seismic studies and site survey data

A significant volume of site survey data has been collected in the drilling area over many years, including multiple generations of two-dimensional (2-D) seismic reflection (e.g., Park et al., 2002), wide-angle refraction (Nakanishi et al., 2002), passive seismicity (e.g., Obana et al., 2004), heat flow (Kinoshita et al., 2003), side-scan sonar, and swath bathymetry data. In 2006, Japan and the United States conducted a joint three-dimensional (3-D) seismic reflection survey over a ~11 km × 55 km area, acquired by PGS Geophysical, an industry service company. This 3-D data volume was used to refine selection of drill sites and targets in the complex megasplay fault region, to define regional structures and seismic stratigraphy, to analyze subsurface physical properties through seismic attribute studies, to expand findings in boreholes to wider areas, and to assess drilling safety (Moore et al., 2007) (Fig. **F3**).

Since 2001, *Shinkai* 6500 dives have revealed a general distribution of cold seeps, surface sediment pore fluid chemistries, thermal structures, and geological structures. Cold seeps are distributed at active faults on the prism slope (Ashi et al., 2002; Toki et al., 2004) and mud volcanoes in the forearc basin, the "Kumano Trough" (Kuramoto et al., 2001). The densest chemosynthetic biological communities are observed along the fault scarp base of the megasplay 30 km southwest of proposed Site NT2-03B. This cold seep site is characterized by high heat flow based on 1 y of monitoring (Goto et al., 2003) and low chlorinity in pore fluid chemistry (Toki et al., 2004), suggesting updip migration of fluids probably through the fault zone from the deep prism. Seafloor observations were also conducted near proposed Site NT2-03B using the submersible *Shinkai* 6500, the JAMSTEC deep-tow video camera 4K, and the ROV *Kaiko*. The gentle slope around proposed Site NT2-03B is completely covered by hemipelagic sediment and shows no indications of any cold seep activity. In contrast to the southern slope of the outer ridge, which was formed by recurrent slip events of the splay fault system, bacterial mats and a carbonate chimney were observed on the landward flank of the outer ridge (Toki et al., 2004). A northeast–southwest elongated depression has developed between the outer ridge and the forearc basin. The deep-towed side-scan sonar system Wadatsumi revealed a strong east-northeast–west-southwest lineament on the basin floor of the depression and a swarm of normal faults at the southern margin of the forearc basin. Bacterial mats, tubeworms, and carbonate crusts were also observed

on the landward slopes of the depression where the forearc basin strata are partly exposed (Lallemant, unpubl. data).

Objectives

Scientific objectives

1. *Acquisition of geotechnical data and establishment of core-log-seismic integration for deep riser drilling.*

Site C0001 (proposed Site NT2-03B) will target the main splay at an ultimate depth of ~3500 meters below seafloor (mbsf) during Nankai Trough Seismogenic Zone Experiment (NanTroSEIZE) Stage 2. Site C0002 (proposed Site NT3-01A) will target the main splay and plate boundary faults at ~3000–4000 and ~6000 mbsf, respectively, during NanTroSEIZE Stage 3. During NanTroSEIZE Stage 1A, a pilot hole was drilled with a total depth (TD) of ~1000 mbsf for riser drilling planned in Stages 2 and 3. Drilling will penetrate the young slope/forearc sediments (hemipelagites and turbidites) in the upper section and obtain the underlying old accretionary prism materials. Acquisition of core and logging data and their integration were geotechnically of primary importance for riser well planning for Stages 2 and 3 and for designing the long-term borehole monitoring system for NanTroSEIZE Stage 4. These pilot holes are important not only geotechnically but also scientifically. In future riser drilling, whole-core recovery is not necessarily guaranteed for two reasons. First, some less scientifically important intervals could be skipped in the interest of saving time. Second, even when attempting to recover whole cores, recovery may be expected to be poor in some sections, especially in highly fractured lithologies. To compensate for incomplete core information, wireline logging and mud logging would be utilized as much as possible to understand lithologic, stratigraphic, geophysical, and geochemical properties of the downhole formations. Therefore, it was of primary importance to establish a complete correlation between the core, log, and seismic data in this pilot hole such as was done in the German Continental Deep Drilling Program KTB, which produced highly successful results (Emmermann and Lauterjung, 1997).

2. *Structural investigations of strain partitioning between the prism and the forearc basin in oblique subduction.*

Defining the upper limit of a splay thrust (Site C0001)

The recent 3-D seismic survey showed that the splay fault system, originally defined on 2-D seismic lines (e.g., Park et al., 2002), is actually composed of two main fault systems referred to as the upper splay fault and the lower splay fault, locally associated with prominent reflectors. The boundary between the slope basin and the underlying locally transparent unit (probably deformed turbiditic sequences) appears in this part of the 3-D box as a high-amplitude reflector with a normal polarity at 200 mbsf. We had working hypotheses for this boundary: a simple sedimentary unconformity between the slope basin and the underlying accretionary sediments, or the updip extension of the upper splay fault. Another interesting structure was a faint landward dipping reflector cutting the slope basin. This reflector possibly corresponded to the updip extension of the upper splay, although no deformation was recognized in the reflectors of the surface basin sediment. Defining the updip extension of the upper splay fault was one of the major structural goals of drilling at Site C0001 during NanTroSEIZE Stage 1A.

Strain partitioning between the active accretionary wedge and the forearc basin domain

Seafloor morphology of the outer ridge domain in the Kumano transect shows numerous linear features. This strongly suggests that it is a strike-slip component of the deformation, which can be interpreted as a strain partitioning of the oblique convergent motion with right-lateral motion mostly expressed along the wedge/forearc boundary. Similar partitioning has been described within the forearc basin of the neighboring Tokai domain (Huchon et al., 1998). Although the main linear depression located landward of the outer ridge might be partly due to erosional processes, it seems to be structurally controlled as shown by a sharp linear scarp seen on the Wadatsumi side-scan sonar images and is probably due to the development of a pull-apart basin. Although the strike-slip component seems to be concentrated mostly on the landward side of the outer ridge, we should carefully check the core-scale structures at Sites C0001 and C0002 for indications of such a strike-slip deformation.

Extensional versus compressive deformation

The Kumano Basin's seaward edge is cut by normal faults with rapidly decreasing spacing toward the outer ridge depression. On the other hand, some minor normal faults can be observed locally just seaward of the lower splay fault. In a working hy-

pothesis that the splay fault moves rapidly during the coseismic period, these features could be related to gravity relaxation of the outer ridge domain during the interseismic period. Observation of such extensional features in a core scale during NanTroSEIZE Stage 1A drilling, as well as their mutual relationships with the compressional structures, would be of primary interest in understanding the deformation cycle of a splay fault system. Structural analyses during IODP Expedition 314, based mainly upon resistivity borehole image analysis, provided northwest–southeast direction compressional and north-northwest–south-southeast direction tensional stress regimes for Sites C0001 and C0002, respectively. We attempted to confirm these stress regimes in core analyses, as well as revealing paleostress regimes recorded in core structures.

3. *Geochemical investigations of migrating fluids through splay faults.*

Geochemistry of pore fluids reflects conditions of the deep prism where structural deformations, diagenesis, and metamorphism occur. Active cold seeps, with bacterial mats and clam colonies, have been observed at the scarp base of the megasplay 30 km southwest of Site C0001 by submersible dives (Ashi et al., 2002). Surface sediment pore fluids are characterized by low chlorinity, low δD, and low $\delta^{18}O$ (Toki et al., 2004). These geochemical and isotopic features prefer land-derived groundwater for their origin; however, it is hard to explain the hydrological connection between land and the seep site 70 km offshore. Seafloor observations with ROV and deep-towed video cameras near Site C0001 have revealed thick hemipelagic cover and no evidence for cold seepage. In shallow cover sediments, diffusion is the dominant mode of upward migration of fluids; however, in the deeper part, channel flow through fault zones and/or fractures may be the dominant mode of fluid migration rather than diffusion with decreasing permeability. Therefore, determining the migrating path of fluids is of primary importance. We penetrated the boundary between the slope basin and the underlying accretionary complex at ~210 m core depth below seafloor (CSF; IODP method A: core expansion lengths overlap [are not scaled]) and obtained pristine fluids from the boundary and the over- and underlying sediments with much less contamination from seawater than sampling at the seafloor. Onshore fluid chemistry analyses will provide valuable information regarding their origins and migrating paths. Integration with fluid chemistries around the lower splay fault and its hanging wall, to be drilled at proposed Site NT2-01B in future NanTroSEIZE expeditions, will help further our understanding of fluid migration.

In contrast to the unidentified source of low chlorinity fluids mentioned above, hydrocarbon analyses indicate a light carbon isotopic composition from dissolved methane and a low C_2H_6/CH_4 ratio, suggesting a biological origin for the methane (Toki et al., 2004). At Site C0002, a clear bottom simulating reflector was located on seismic profile at ~400 mbsf. We are also interested in understanding the relationships between formation and migration of methane and sediment deformation. Formation and dissociation of methane hydrates probably affect methane circulation.

4. *Reconstruction of the prism and the forearc basin evolution based on stratigraphic records.*

Surface strata at Site C0001 were expected to consist of reworked sediments and hemipelagite. A piston core sample taken from the base of the fault scarp 30 km southwest of Site C0001 included >10 debris layers intercalated with hemipelagic sediments, suggesting repeated falling or sliding at the time of fault displacement and/or a nearby earthquake. The recurrence time of probable event depositions was estimated to be ~1000 y between 15 and 27 k.y. ago based on carbon isotope ages of foraminifer fossils (Ikehara, unpubl. data). A similar sedimentary sequence was expected in the shallow part of Site C0001, which provides longer records of recent activities of the megasplay faults. On the other hand, the upper 920 m strata at Site C0002 was expected to consist of alternation of hemipelagites and turbidites. Drilling at Site C0002 covered most sequences of the Kumano Basin, although its deepest parts were missing. High-resolution bio- and magnetostratigraphies provided age constraints to several unconformities, which may reveal that the history of the basin evolution correlated with the megasplay fault system activity.

Old accreted sedimentary sequences were expected beneath the boundary at 200 mbsf for Site C0001 and 920 mbsf for Site C0002. These accreted sequences are characterized by transparent acoustic features in 3-D seismic profiles at Site C0001. At Site C0002, these sequences are characterized by a stack of strong but discontinuous reflectors. These features are interpreted as highly dipping bedding reflectors and/or highly disrupted sequences. Microfossil age determinations, thermal histories from clay diagenesis, and fluid inclusion thermobarometries in quartz and calcite veins could provide information about the growth and exhumation of the accretionary prisms.

Strategy

Diagenetic processes, microstructures, chemical compositions, bio- and magneto-stratigraphies, and potential sealing/healing processes were examined in the accretionary prism and the overlying slope/forearc basin sediments. Physical property data, including porosity, electric resistivity, and seismic velocity, were key parameters in assessing mechanical and hydrologic behaviors and for core-log-seismic integration. Whole-round and discrete core sampling are necessary for postexpedition studies, such as permeability and consolidation experiments and mechanical (rock friction and triaxial) tests. Pore fluid chemistry data will be important in constraining the hydrologic behavior of faults and unconformities and the source of any chemically and/or isotopically distinct deeply sourced fluids. Expected lithologies from seismic and logging data were hemipelagite and slump deposits for the upper ~200 m section and well-consolidated and highly deformed sediments in the underlying accretionary prism section. We were also expecting to encounter fault rocks that were cataclastically deformed to various extents.

During Expedition 314, LWD holes had already been drilled at Sites C0001 and C0002. In addition, a pilot hole and a short geotechnical hole (~30 m) were also drilled at Site C0001. We planned two more holes for coring at each site during this expedition. At Site C0001, the first hole was to be cored with the hydraulic piston coring system (HPCS)/extended shoe coring system (ESCS) to refusal depth. Refusal depth was estimated as ~600 mbsf in the original plan described in the Expedition 315 *Scientific Prospectus* (Ashi et al., 2007); however, we had to modify the depth to ~200 mbsf based upon our experience during Expedition 314. After refusal, we planned to drill a new hole for rotary coring. During Expedition 314 we encountered a zone of drilling difficulty at ~450–600 m CSF. Unstable borehole conditions were expected in this so-called "sticky zone." Therefore, we planned to stop rotary core barrel (RCB) coring just above this zone and drill through it with a normal drilling assembly and then restart coring from 600 mbsf. We planned to core the skipped intervals with a 4 inch petroleum-type coring system after reaching TD (1000 mbsf) (Fig. **F4A**). We prepared a sufficient amount of bentonite Hi-Vis mud and weighted kill-mud for potential overpressure.

Site C0002 was one of the high-priority global contingency sites. Because the riser top-hole casing operation during Expedition 315 was cancelled, we had plenty of time to drill/core another site. Based on the opinion of the expedition's riser pilot, our primary targets were the accretionary prism and its upper boundary to the overlying

forearc basin. For this reason, we started coring from 475 mbsf, aiming for TD (1400 mbsf), and allocated the remaining days for shallow coring with the HPCS (Fig. **F4B**).

Estimating the geothermal gradient was one of the key issues for future deep riser drilling. The advanced piston corer temperature tool (APCT3) was used to measure in situ formation temperatures. The APCT3 is generally used every 30 m for HPCS coring intervals.

Principal results

Site C0001

Site C0001 (proposed Site NT2-03) is located on the hanging wall of the megasplay fault where future riser drilling is planned to 3.5 km depth. LWD data taken during Expedition 314 in Hole C0001D delineated four lithologic units (Units I–IV, from top to bottom) and northeast–southwest borehole breakouts suggesting a northwest–southeast compressional stress field (Kinoshita et al., 2008).

Coring in Holes C0001E and C0001F was conducted from the seafloor to 248.8 m CSF with the HPCS and ESCS. ESCS coring recovered only two cores because of severe drilling disturbance. RCB coring was done from 230.0 to 458.0 m CSF in Hole C0001H. Bad hole conditions did not allow continued coring to the original TD of 1000 mbsf. In addition to cores recovered during this expedition, we also described and analyzed Hole C0002B cores (~30 m long) recovered during Expedition 314. These cores were taken for geotechnical investigations for future riser well planning and remained unprocessed after nondestructive whole-round measurements and whole-round core sampling were completed.

We identified two lithologic units at Site C0001 (Fig. **F5**). Unit I is Quaternary to late Pliocene in age and extends from the seafloor to 207.17 m CSF. The dominant lithology of Unit I is silty clay and clayey silt. Secondary lithologies include thin interbeds and irregular patches of sand, sandy silt, silt, and volcanic ash. Overall, the siliciclastic interbeds define a trend of fining and thinning upward. Unit I can be divided into three subunits based on grain size, layer thickness, sedimentary structures, trace fossils, and mineralogy. Subunit IA extends from the seafloor to 168.35 m CSF. The dominant lithology is structureless greenish gray to grayish green mud with local wavy and dark green laminae. The most common interbeds consist of white or light gray to dark gray volcanic ash. Subunit IB extends from 168.35 to 196.76 m CSF. The sub-

unit boundary is defined by the first occurrence of multiple closely spaced silt beds. The dominant lithology is greenish gray to grayish green mud. Dark gray silt to sandy silt is the characteristic minor lithology of this subunit. These thin beds display sharp bases, faint plane-parallel laminae, normal size grading, and diffuse tops. Such features are typical of fine-grained turbidites. Subunit IC extends from 196.76 to 207.17 m CSF. The dominant lithology is gray to dark bluish-gray sand, intercalated sporadically with greenish gray to grayish green mud. Grain size varies from silt to medium sand but is predominantly fine sand. Unconsolidated sand appears to be structureless and soupy, but this is probably an artifact caused by coring disturbance. Bed thickness is impossible to recognize because of flow within the core liner. The sand grains consist mostly of detrital quartz and feldspar with abundant sedimentary and low-grade metasedimentary rock fragments.

The boundary between Units I and II is an unconformity, with an associated hiatus, as shown by both paleomagnetic and biostratigraphic data. Strata below the unconformity are late Pliocene to late Miocene in age and extend from a depth of 207.17 m CSF to the bottom of Hole C0001H at 457.8 m CSF. Within Unit II, three subunits were recognized based on LWD data, but lithologic variations in the cores are not distinctive enough to warrant subdivision on the basis of texture, composition, or sedimentary structures. The dominant lithology of Unit II is greenish gray to grayish green bioturbated mud. The mud contains local wavy laminae, as defined by darker green color and higher clay content. Pyrite grains are moderate to abundant.

Cores taken from Holes C0001B, C0001E, and C0001F were cross-correlated based on whole-round multisensor core logger (MSCL-W) magnetic susceptibility data. The interval below 6 m CSF in Hole C0001B correlates with the 1.5 m deeper interval of Hole C0001E, although there seems to be no shift at the core top. The lowermost core in Hole C0001E and the uppermost core in Hole C0001F overlap. A distinctive pair of magnetic susceptibility peaks, corresponding to ash layers, indicates a 2.7 m deeper offset of Hole C0001F to Hole C0001E. The intercalated mud intervals between 196.76 and 206.93 m CSF in cores from Hole C0001F are well imaged as conductive layers in the resistivity-at-the-bit image between 192 and 199 m logging-while-drilling (LWD) depth below seafloor (LSF) in Hole C0001D. This imaging constrains the stratigraphic offset between Holes C0001E and C0001D to 4.75 m at the top of the sand and 8 m at the base. A good fit between the MSCL and LWD gamma ray data is obtained in the lower part of Hole C0001D with offsets of 7–9 m. This suggests a lateral variation of sand thickness from 7 m in Hole C0001D to ~10 m in Hole C0001F. Taking into account this 7 m shift of the base of Hole C0001F, it is logical to fit the

magnetic susceptibility peaks at 231.08 and 233.04 m CSF in Hole C0001H with those located ~8 m deeper at 239.49 and 240.37 m CSF in Hole C0001F and to infer an upward shift of ~1 m of the uppermost part of Hole C0001H with respect to the LWD hole (C0001D).

Nannofossils and planktonic foraminifers were recovered from the sedimentary succession at Site C0001. The combined results suggest that there is at least one time break in the sequence in the interval from the late Quaternary to the Miocene/Pliocene boundary. Foraminifers and nannofossils are generally abundant within Subunit IA, with preservation ranging from moderate to good; best preserved assemblages are found in the Pleistocene section. The Pliocene/Pleistocene boundary is placed at ~190 m CSF based on planktonic foraminiferal evidence. The existence of Pliocene nannofossil assemblages just below this depth is consistent with the foraminifers defined. A marked change in both nannofossil and foraminifer assemblages occurs in the interval between 207.43 and 213.39 m CSF; mixed assemblages of late Pliocene to late Miocene age were encountered. The Miocene/Pliocene boundary is placed below 419.5 m CSF based on foraminiferal evidence. Nannofossil results, however, suggest that the boundary is located between 448 and 458 m CSF. The exact position of the Miocene/Pliocene boundary at Site C0001 remains equivocal and warrants more detailed investigation.

Natural remnant magnetization was measured at 5 cm intervals in each core section, followed by alternating-field (AF) demagnetization at 5, 10, 15, and 20 mT peak fields. Cores from Hole C0001H (240–458 m CSF) were excluded because of the lack of intact sections long enough for pass-through magnetometer analysis. The polarity pattern was determined by the magnetic inclination after AF demagnetization at 20 mT (Fig. F6). The magnetic polarity record was then identified using biostratigraphic datums and correlated with the Geomagnetic Polarity Time Scale of Gradstein et al. (2004). In Hole C0001E, the magnetic inclination is dominantly positive above 86 m CSF. A polarity change from normal to reversed at this depth is interpreted as the Brunhes/Matuyama Chron boundary, in agreement with the identified nannoplankton zone. The Matuyama Chron (C1r) is characterized by the predominance of reversed polarity. A short normal polarity interval observed between ~127 and ~131 m CSF is interpreted as a part of the Jaramillo Subchron (C1r.1n), although the upper and lower limits are missing. In Hole C00001F, we could reliably determine the top of the Olduvai subchron (C2n) at 174.7 m CSF. The bottom of the Olduvai occurs at 193.5 m CSF, although the subsequent older Matuyama Chron is only represented by 3.3 m of

sediment. Below, we encountered thick sandy Subunit IIB, which is completely disturbed, preventing any continuous reliable paleomagnetic analysis.

More than 550 individual structural features were documented and described. Most of these features were reoriented to a geographic reference frame using shipboard paleomagnetic data. The main features were faults, shear zones, vein structures, breccia, and steepened bedding. Faults are relatively planar narrow zones of deformation characterized by a single band of concentrated deformation that is slightly bright in X-ray CT images, suggesting a higher density than the adjacent wall rock. Shear zones (or deformation bands) are generally wider than faults and are often composed of multiple sets or bands of concentrated deformation. Vein structures include a variety of structures, many of which have been recognized during previous ocean drilling and have been interpreted as dewatering structures. This category of structures includes the classic sigmoidal-shaped suite of thin mud-filled veins originally described by Ogawa (1980) and Cowan (1982). Breccia is marked by a relatively high concentration of small polished and slickenside lens-shaped fragments of clayey silt or silty clay a few centimeters to 2 dm in thickness. Figure **F7** shows the vertical distribution and dip angle of the dominant deformation structures at Site C0001. Bedding generally dips gently with only three anomalous zones: (1) ~80–100 m CSF, (2) 140 m CSF, and (3) ~210 m CSF. Faults generally occur at all depths at Site C0001, but only normal faults and a few relatively minor thrust faults occur above the zone of deformation at 220 m CSF. A cluster of normal faults is present in the interval 150–160 m CSF (Fig. **F7**), just above the breccia zone. The orientations of faults strongly contrast above and below the highly deformed zone at 220 m CSF. In the slope apron and above the deformed zone, 90% of the faults described are conjugate sets of normal faults dipping at 60° and striking southeast, indicating northeast–southwest extension. Exceptionally, a few thrust faults dipping at 50° encountered just above the deformed zone suggest northwest–southeast shortening. The geometry and kinematics of planar structures display greater variation below the deformed zone. The fault plane solutions computed from normal and thrust faults are respectively consistent with the northeast–southwest extension and northwest–southeast shortening.

A total of 48 whole-round sections were collected for interstitial water analyses from Holes C0001E, C0001F, and C0001H. Routine sampling density was approximately one per core; denser sampling was done from the first core just below the seafloor (three samples), where the considerable mixing of interstitial water with seawater and anaerobic methane oxidation occur. SO_4 concentration decreases linearly from the seawater value at a rate of ~2.5 mM/m to nearly 0 mM at 14 m CSF at Site C0001. Al-

kalinity and dissolved PO_4 concentration consistently increase to maximum values at ~50 m CSF, reflecting the activity of interstitial microbes that metabolize sedimentary organic matter through a reaction that ultimately produces inorganic metabolic by-products in the shallow interval (e.g., Berner, 1980). Dissolved NH_4 concentration also reaches a maximum constant value between 105 and 175 m CSF, resulting presumably from anaerobic deammonification of organic matter during early diagenesis in this interval. The concentration of Cl rapidly decreases from the seafloor to 100 m CSF to a local minimum and then increases continuously below this depth (Fig. F8). Chlorine is one of the most conservative elements in marginal settings; therefore, the 3.6% dilution at 100 m CSF reflects input of freshwater. The coincidence of the Cl minimum with the NH_4 maximum at 100 m CSF suggests that water input from a deammonification reaction could be responsible for this freshening. This question will be resolved by future oxygen and hydrogen isotopic analysis, which may record the presence of hydrate-sourced fluids as another candidate. Sodium concentration is scattered because of analytical error, but there is a slight increase in concentration with depth and a clear decrease at the seafloor (Fig. F8). The monotonous decrease of K with depth is the result of continuous reaction with clay mineral phases in thermal equilibrium. There is a pronounced breakout of the trend at 112 m CSF, resulting from interaction with a volcanic ash layer. There is also a localized minimum in Mg and maximum in Ca concentration at this depth. The increase in Ca at greater depths suggests that Ca is being released from clay minerals at all depths, but the amount of removal exceeds the amount of production in the upper zone.

Concentrations of methane, ethane, and their ratio (C_1/C_2) are shown in Figure F9. Methane concentration increases rapidly from 3.7 ppmv in the near surface to 37,204 ppmv at 34 m CSF. It decreases downhole to 100 m CSF and remains constant until 231 m CSF. Below this depth, methane concentration shows wider variation but is relatively high on average; the highest value occurs at 278 m CSF. Vertical distribution of ethane is similar to that of methane. C_1/C_2 ratios gradually decrease with depth in Unit I and slightly increase with depth in Unit II. The increase of methane concentration and C_1/C_2 ratio in Unit II indicate contribution of biogenic methane. The majority of C_1/C_2 ratios >1000 suggests that the methane at Site C0001 is of biogenic origin. Initial results for calcium carbonate ($CaCO_3$), total organic carbon (TOC), organic carbon to total nitrogen (C/N) ratio, and total sulfur in the sediments are presented in Figure F9. Calcium carbonate, TOC, and C/N ratios generally decrease with depth in Unit I and remain constant in Unit II except for some high values of TOC and C/N ratio below 375 m CSF. Total sulfur content is fairly uniform with two spikes at 103 and 181 m CSF and a cluster showing high values between 200 and 260 m CSF.

Whole-round cores were taken from Holes C0001E, C0001F, and C0001H for micro-biological analysis. Some of the whole-rounds were subsampled on board for cell fix-ing, deoxyribonucleic acid (DNA) and ribonucleic acid (RNA) extraction, and culturing studies. A large part of the microbiological work will be done on shore. Se-lected samples of fixed cells were stained on board with double-stranded DNA-bind-ing SYBR green-I-stain. Cells were detected in core samples from 0.5 to 448 m CSF. More than 200 enrichment cultures were established with the aim to culture sulfate-reducing microorganisms. The cultures were monitored for sulfate reduction based on the formation of black iron sulfide precipitate. During the expedition, blackening of the growth medium was observed in only a few sediment cultures incubated at 9° or 37°C and in drilling fluid (seawater gel) cultures incubated at 37°C.

Moisture and density (MAD) was measured on discrete subsamples collected from working-half cores as well as from "clusters" adjacent to whole-round samples (Fig. **F10**). MAD porosity gradually decreases with depth throughout Subunits IA and IB. Subunit IC shows extremely low porosity, probably due to a highly disturbed sandy sequence. There is a large gap of porosity between Subunit IC and Unit II. The entire porosity profile in Unit II is shifted higher than those of Subunits IA and IB. The cause of this shift is not evident and should be resolved in terms of different backgrounds of compaction and digenesis of both units. Wet bulk density data show a reverse cor-relation with porosity data. Grain density values show no specific trend with depth, although there is subtle lack of low values at Subunit IB. Undrained shear strength measurements were determined using a miniature vane shear device and a pocket penetrometer. Shear strength increases with depth except for some low values below 228 m CSF. These data are derived from ESCS core samples, suggesting heavy drilling-induced disturbance. Thermal conductivity measured on whole-round samples from HPCS cores (<230 m CSF) and on split samples from RCB cores (>230 m CSF) are widely scattered but generally increase with depth.

Downhole temperature measurement was conducted at seven depths with the APCT3 in Holes C0001E and C0001F. Measurement was done on every third core from 13.6 to 170.98 m CSF. Temperatures increase almost linearly with depth with a gradient of ~0.042°C/m.

Site C0002

Site C0002 is located at the southern margin of the Kumano forearc basin where fu-ture riser drilling to 6 km depth is planned. LWD data of the thick forearc basin se-

quence and the top of the underlying accretionary prism were obtained in Hole C0001A during Expedition 314 and identified four lithologic units: Units I–IV (Kinoshita et al., 2008).

Coring in Hole C0002B was conducted from the middle of the forearc basin (475 m CSF) to the top of the accretionary prism (1057 m CSF). Hole C0002D was mainly dedicated to geotechnical assessments to 70 m CSF for future riser drilling. After recovering these cores, we continuously cored to 129.15 m CSF and conducted spot coring at 150 and 200 m CSF in the same hole. Only time-critical whole-round sampling and minimum measurements were conducted, such as pore fluid geochemistry, X-ray CT scan, MSCL-W, MAD, and thermal conductivity. In order to complement missing intervals by dense whole-round sampling in the upper 10 m, we took two cores in Hole C0002C to 13.77 m CSF. Therefore, data presented here are mainly from Hole C0002B cores.

Three lithostratigraphic units were identified in cores taken from below 479.40 m CSF in Hole C0002B on the basis of grain size, layer thickness, sedimentary structures, trace fossils, and mineralogy (Fig. **F11**). Core recovery was generally poor to moderate and was particularly bad within intervals in which the log character was indicative of high sand content. We therefore adopted positions of unit boundaries determined by LWD during Expedition 314 (Kinoshita et al., 2008). Hole C0002B is located 60 m south–southwest of Hole C0002A for LWD. The forearc basin sequence has a dip of 6.5° to 7.0°; hence, a stratigraphic offset of 6.0 to 7.5 m is expected between the boreholes in Lithologic Unit II. Core-log integration between LWD bit resistivity and core resistivity of discrete samples shows a 11–12 m deepening of forearc basin strata from Hole C0002B to Hole C0002A.

The dominant lithology of Unit II is greenish gray to grayish green mud (silty clay to clayey silt). Secondary lithologies include thin interbeds and irregular patches of sand, sandy silt, silt, and rare volcanic ash. The mud is locally structureless but more commonly shows plane-parallel laminae and incipient fissility. Orientation of this fabric is horizontal to gently inclined. Dark gray silt, sandy silt, and silty sand are the characteristic interbeds of Unit II. These beds are typically <5 cm thick and display sharp bases, faint plane-parallel laminae, normal size grading, and diffuse tops. Such features are typical of fine-grained turbidites.

The boundary between Units II and III is defined by a shift in lithofacies from turbidites above to condensed mudstone below at 830.4 m LSF (Kinoshita et al., 2008). The

2008). The dominant lithology of Unit III is greenish gray, gray, and gray-brown mudstone. Mud texture is finer grained than equivalent deposits in Unit II, and bioturbation is more widespread and diverse. Secondary lithologies are limited to sparse beds and irregular lenses of volcanic ash. Locally, sharp-topped zones with glauconite grains suggesting erosion and reworking of compacted and/or cemented clay-rich sediment were observed.

The boundary between Units III and IV, an unconformity between the forearc basin and the accretionary prism, is defined by a change in structural style and a shift in lithofacies from a condensed mudstone section above to interbeds of mudstone, siltstone, and sandstone below. As defined by log character, the unit boundary is positioned at a depth of 935.6 m LSF. The dominant lithology of Unit IV is gray to greenish gray and dark gray mudstone. The mudstone contains local wavy laminae or bands, as defined by darker green color and higher clay content. Thin layers of siltstone are rare. Sandstone also occurs locally, and in some cases the sand is cemented by calcium carbonate.

The preliminary biostratigraphy for Site C0002 is based on calcareous nannofossils. Nannofossils are continuously present throughout the sequence. Although the nannofossils significantly decrease in abundance downhole, a good biostratigraphic framework could be established for the entire succession. Nannofossil assemblages recovered from Unit II are Pleistocene in age. Unit III comprises a suite of Pliocene biostratigraphic events. In Unit IV sediments, only one nannofossil event was identified, assigning this unit a late Miocene age.

Remnant magnetization measurements on archive-half cores from Hole C0002B above 620 m CSF suggest artificial overprints. Excluding these intervals, the magnetic polarity record after AF demagnetization at 30 mT was correlated to the Geomagnetic Polarity Time Scale of Gradstein et al. (2004). A clear polarity change from negative to positive inclination was observed at ~850 m CSF. Referring to the biostratigraphic datum, this reversal can be correlated to the top of Olduvai and the reversed polarity above this horizon can be correlated to Matuyama Chron. Magnetic inclination values also infer tectonic tilting of bedding planes after acquisition of remnant magnetizations. Measurements of bedding dips on split cores show a gradual increase from Unit II to Unit III and steeper dips in Unit IV with high scattering distribution (Fig. F12). The inclination value in the Unit II interval is relatively close to the inclination estimated from the site latitude. In contrast, the Unit III interval reveals a significantly steeper inclination, suggesting northward (northwest–northeast) tilting of

strata. Magnetic inclination in Unit IV ranges more widely toward both lower and higher angles. The wide variety of dip and azimuth in Unit IV is consistent with highly deformed strata of the accretionary prism expected from seismic reflection profiles.

More than 400 structural features were observed in cored sediments. Five main structural features and one subordinate feature were identified. The main features observed were steepened bedding, faults, breccias, shear zones, and vein structures. Fissility occurred only in the upper sections of Hole C0002B and was consistently oriented parallel to bedding. Vein structures are particularly well developed in Unit III. A wide variety of forms and shapes were observed for vein structure; however, most of them are perpendicular to the bedding. Faults are relatively rare in the upper 500 m of Hole C0002B. Although a small cluster of moderately dipping faults occurs at ~700 m CSF, most of the observed faults occur in two clusters below 900 m CSF (Fig. **F12**). One cluster ranges from 920 to 950 m CSF, whereas the other cluster more widely ranges from 1000 to 1050 m CSF within Unit IV. About 20% of the planar and linear features observed in the cores were reoriented to true north using nearly 50 individual paleomagnetic poles. Three deformation phases were suggested by textures and crosscutting relations. An early phase of thrust faulting (and possibly strike-slip faulting) exhibits northwest–southeast shortening. Two phases of normal faulting occurred subsequent to thrusting. The first is recorded in shear zones and indicates northeast–southwest extension. The second is recorded in normal faults and indicates north–south extension.

A total of 31 whole-round samples were collected for interstitial water analyses from Hole C0002B on a routine bases with a frequency of approximately one per every core. Sulfate concentration generally ranges between 1.0 and 4.0 mM, well above the detection limit throughout the entire interval (Fig. **F13**); even potential contamination of drilling fluid is taken into consideration. These concentrations suggest existence of high sulfate fluids at greater depths, inferred from previous studies (e.g., ODP Sites 1173, 1174, and 1176A; Moore, Taira, Klaus et al., 2001). Alkalinity and ammonium concentrations decrease steeply downhole, showing inflections at unit boundaries. We infer that the lithologic boundaries affect fluid migration and/or reaction. Salinity and concentrations of chlorine consistently increase downhole from levels below seawater value at ~800 m CSF and then slightly decrease toward the bottom of the hole (Fig. **F13**). Dilution at the top of the cored interval (475 m CSF) is also observed in all other cation profiles, indicating the presence of a freshwater source or path above this interval. A coupled change in concentrations of sodium, potassium,

and calcium across 800 m CSF may suggest a progressive reaction of fluid with clay minerals through Units III and IV or deeper, probably a result of smectite illitization (Fig. F13).

Concentrations of methane, ethane, and propane are shown in Figure F14. Methane concentration is constant to 610 m CSF and increases throughout the rest of Unit II. It decreases with depth in Unit III and remains low in Unit IV except for high values at the bottom of Hole C0002B. Propane was also detected in the lower part of the hole. C_1/C_2 ratios below 900 m CSF suggest some contribution of thermogenic hydrocarbons. Initial results for inorganic carbon, $CaCO_3$, TOC, total nitrogen, C/N, and total sulfur in the sediments are presented in Figure F14. $CaCO_3$ concentration is significantly high in Unit III. C/N ratios suggest that organic matter in sediments is mainly of marine origin. Total sulfur content is constant in Unit II, increasing with depth in Unit III and showing high values with scattering in Unit IV.

Whole-round cores were taken from Holes C0002B and C0002D for microbiological analysis. Some of the whole-round cores were subsampled on board for cell fixing, DNA and RNA extraction, and culturing studies. A large part of the microbiological work will be done on shore because of time constraints and the need for special laboratory facilities. Onboard work mainly included preserving the whole-round cores and subsamples for shore-based research, fixing cells for cell detection and counting, and setting up enrichment cultures of sulfate-reducing bacteria. Selected samples of the fixed cells were stained on board with double-stranded DNA-binding SYBR green-I-stain. Cells were detected in core samples to 1020 m CSF.

MAD was measured on discrete subsamples collected from the working-half cores as well as from "clusters" adjacent to whole-round samples (Fig. F15). Porosity gradually decreases with depth within Unit II, remains constant in Unit III except for a shift to higher values in the lower part of the unit, and increases between 1005 and 1050 m CSF in Unit IV. Thermal conductivity was measured on whole-round core sections above 555 m CSF (needle probe method) and on split working-half cores (half-space method) for stiffer sediments below. Thermal conductivity values increase with depth in Unit II and show no specific trend in Unit III. The decrease of thermal conductivity below 1000 m CSF is consistent with the increase in porosity. Shear strength experiments using a penetrometer above 641 m CSF show highly scattered values, suggesting strong core disturbances caused by RCB coring.

Six measurements of downhole temperature were conducted with the APCT3 in Hole C0002D. The measurement interval is every second core above 72.38 m CSF. Measurements were also conducted at 110.38 and 158.97 m CSF. Temperature increases almost linearly with depth with a gradient of ~0.043°C/m.

Summary and implications

Expedition 315, entitled "Megasplay Riser Pilot," was planned as one of the NanTroSEIZE Stage 1A expeditions for the future deep riser drilling of the megasplay fault in NanTroSEIZE Stage 2. The primary engineering and scientific objectives of this expedition were to obtain geotechnical information needed for well planning of future riser drilling to 3500 mbsf. The location of Site C0001 is critical for understanding the nature of the shallow portions of splay faults. The scientific targets of this expedition were stress regime and deformation mechanics, fault-related fluid source and migration pathways, and correlations between fault activity and slump deposits on the trench slope.

Site C0001 is located at the small bench on the hanging-wall of the megasplay fault (the lower splay fault) and the footwall of the subsidiary fault (the upper splay fault). 2-D and 3-D seismic profiles show that the small slope basin with a ~200 m thick series of layered reflectors is developed, overlying the more transparent unit corresponding to the wedge-shaped seaward edge of the hanging-wall. Coring revealed that the slope basin is composed mainly of Quaternary to late Pliocene silty clay and clayey silt with numerous intercalations of volcanic ash layers. The bottom of the basin is composed of a thick sand layer which overlays the late Pliocene to late Miocene transparently and probably belongs to the accretionary prism unit. The beginning of the slope basin sedimentation defines the age of the change from the active compressional deformation in the accretionary prism deformation around Site C0001 to an extensional deformation mode. We could not find any definite candidates for a deformation zone corresponding to the seaward extension of the upper splay fault. In contrast, normal faults are dominant in the slope basin and are clustered at some depths. Deformations along the upper splay fault seem to be more complex than those expected in the Expedition 315 *Scientific Prospectus* (Ashi et al., 2007). Further detailed analyses on deformation structures are needed for understanding the development of this complex wedge-shaped basin. The *Scientific Prospectus* also anticipated a geochemical signal through the splay fault. Preliminary results of shipboard pore

fluid geochemistry, however, indicated no specific fluid signal except for some gaps at the lithologic unit boundaries, suggesting minor fluid flow and/or diagenesis.

Minor faults, mostly recognized as dark-color seams, were pervasive in clayey sediments and mudstone of entire intervals. Structural analyses of such fault planes and slickenlines were crucial for estimating changes of paleostress fields. Our preliminary results suggest that the direction of the maximum horizontal compressive stress remains northwest–southeast throughout the entire interval; changes of vertical stress exhibit normal faults in the shallow formation and reversed and strike-slip faults in the deep formation. These observations are consistent with results from the northeast–southwest borehole breakouts observed by LWD during Expedition 314 (Kinoshita et al., 2008) and provide more detailed constraints on the stress field in the trench slope site.

Site C0002 is located at the southern margin of the forearc basin. Age determination of the forearc basin sedimentation overlying the accretionary prism is critical to the estimation of the beginning and activities of the splay fault. Site C0002 penetrated Quaternary alternation of fine-grained sandstone and mudstone and basal Pliocene mudstone and cored the late Miocene accretionary prism rock to 1057 m CSF. Facies analysis revealed rapid sedimentation in the forearc basin during the Quaternary and sediment-starved conditions in the basal slope basin during the Pliocene. Further details of evolution of the forearc basin and accretionary prism will be clarified by integration of shipboard and shore-based studies. Pore fluid geochemistry showed that concentrations of most analyzed elements were strongly controlled by lithologic boundaries. Further shore-based studies including isotopes are needed for better understanding of the fluid migrations and/or reactions.

Deformation structures such as steepened bedding, faults, breccia, shear zones, and vein structures were observed. Although the number of fault analysis was limited because of low core recovery and a shortage of structural geologists during replacement of shipboard scientists, we could determine the change of the stress field:

1. First phase of northwest-southeast shortening by thrust faulting and possibly strike-slip faulting,
2. Second phase of northeast–southwest extension by normal faulting, and
3. Third phase of north–south extension by normal faulting.

The last phase showed good correlation with borehole breakouts observed with LWD. The recovered core samples record more details about stress fields as well as their historical changes.

A large contrast in stress condition between Sites C0001 and C0002 was predicted in our *Scientific Prospectus* (Ashi et al., 2007) as a strain partitioning along the boundary between the forearc and the accretionary prism domain. Determining the cause of this contrast will be a goal of shore-based studies. Furthermore, coexistence of normal and reverse faults mentioned in our *Scientific Prospectus* may imply changes of stress conditions during the seismic cycle. Postexpedition investigations could provide significant information for determination of such deformation histories.

Downhole temperature measurement using the APCT3 was first applied to the *Chikyu* expedition and successfully conducted to 171 m CSF at Site C0001 and to 159 m CSF at Site C0002. Results of downhole temperature measurements yielded almost linear downhole increases in the range of measured depths. Downhole measurement provides better information about temperatures at great depths than conventional type near-surface heat flow measurements, which are highly affected by fluctuation of seafloor temperature. Acquisition of a good temperature profile and thermal conductivity data are crucial for future deep well planning and the mechanical design of long-term borehole tools to be installed during NanTroSEIZE Stage 4.

Preliminary scientific assessment

Expedition 315 started on 16 November 2007, one day earlier than originally planned. Before the start of coring, we established a core processing flow largely different from previous ODP and IODP expeditions, mainly because of extensive whole-round core sampling. Our basic strategy was to take whole-round core samples while avoiding disturbing structurally and sedimentologically important layers. We cut whole-round cores for interstitial water analyses at the core cutting area and took X-ray CT scan images immediately, as they had precedence over other core sections. After real-time screening of internal structures by a sedimentologist and a structural geologist, whole-round cores were squeezed for geochemical studies. Whole-round core samples for microbiology were taken just after X-ray CT scanning and before MSCL-W measurements. Other less time-critical whole-round core samples, such as those taken for geomechanical, structural, and physical property purposes, were cut after MSCL-W measurements. These samples were carefully chosen based on screening by

X-ray CT scan images. This routine satisfied both good quality whole-round core sampling and protection of structurally and/or sedimentologically important horizons. The process resulted in a complex core flow and in fact caused some confusion in core processing at the beginning; however, it worked very effectively once it was well established.

HPCS coring in stiff formations often caused twisting or burst core liners; however, the cause is still unidentified. Because penetration of HPCS coring was poor, we conducted ESCS coring. Nevertheless, we stopped it for two cores because of severe biscuiting that prevented our taking any decent quality samples for physical properties, even though recovery rates were high. RCB coring was then performed in Hole C0001H; this first attempt on the *Chikyu* was successfully conducted from 240 to 458 m CSF, although recovery was generally as low as 30%–40%. We stopped coring just above the "sticky zone" intervals in which LWD operation during the previous expedition had met with difficult borehole conditions. We washed out this zone and attempted to restart coring at 600 m CSF. We could drill through the sticky zone without any major drilling problem; however, borehole conditions became worse with time and we finally gave up coring below the sticky zone. It was a disappointment not to obtain any samples from within and below the sticky zone because different features were presented in LWD data from the accretionary prisms above and below this zone. The nature of the sticky zone still remains unclear. Regarding the change in stress state between the hanging wall and footwall interpreted from resistivity images, it is likely to be a group of small faults or a fault swarm. Although we could not reach the original target depth, we obtained a complete data set of both slope basin sequences, including a thick basal sand layer and part of the underlying accretionary prism. High resistivity and low gamma ray horizons frequently intercalated with mud were interpreted as turbidites during Expedition 314; however, most of them were in fact volcanic ash layers.

The original plan after coring at Site C0001 was a casing operation for 3.5 km riser drilling during NanTroSEIZE Stage 2. The casing operation was postponed, however, because of the strong Kuroshio Current, which sometimes exceeded 5 kt. As a consequence, the 12 days planned for the casing operation were used for science. There were several contingency sites in the Expedition 315 *Scientific Prospectus* (Ashi et al., 2007), including input sites seaward of the trench axis (proposed Sites NT1-01 and NT1-07), slope basins to study slope instability caused by splay fault activities (proposed Sites NT2-05 and NT2-10), and the Kumano forearc basin and underlying ac-

cretionary prism (proposed Site NT3-01). We chose the last one for the following reasons:

- The site is a future 6 km riser site (NanTroSEIZE Stage 3), and obtaining geologic and geotechnical information from the shallow part of the accretionary prism and the overlying sedimentary sequences fits the primary expedition goal of "riser pilot" study.

- Paleostress reconstruction in the forearc basin and comparison with results from Site C0001 aid our understanding of the changes of stress fields associated with the splay fault system.

- A complete data set of LWD data to 1400 m CSF were taken during Expedition 314 that enables core-log (and seismic) integration and provides more useful information than that gained by coring only.

- Sedimentation history of the forearc basin is key information for elucidating the relationships between the accretionary prism growth and the evolution of the splay fault system.

We did not have enough time for coring of entire intervals to TD at Site C0002. Because our primary target was the shallow portion of the accretionary prism and the boundary to its overlying forearc basin, we started coring at 475 m CSF in order to reach TD within the expedition schedule. As was expected from LWD results, we encountered many thick sand layers in the forearc basin sequences. However, their actual occurrence was far less than expected from LWD data. The poor RCB core recovery rate (average = 35%) suggests selective omission of loose sand layers. Coring was successfully conducted through the unconformity between the forearc basin sequence and the accretionary prism at ~920 m CSF and continued to 1057 m CSF. Depositional ages were considerably well determined by micropaleontological and paleomagnetic investigations.

We had to stop coring in Hole C0002B at 1057 m CSF because of bad borehole conditions. As there were still several days remaining, we determined to conduct further coring in the shallow part of the forearc basin. Our main purpose was a geotechnical assessment of the riser tophole section to 70 mbsf. Coring and downhole temperature measurement were conducted in Hole C0002D to 204 m CSF. Before drilling Hole C0002D, a short (13.77 m) hole (C0002C) was cored. Two cores, mainly dedicated to fluid geochemistry and microbiology, were cut just beneath the seafloor to compensate dense whole-round sampling from Hole C0002D. Cores from Holes C0002C and

C0002D were stored in the cold reefer without splitting after nondestructive whole-round measurements and sampling.

Expedition 315 was originally scheduled as a short expedition: 21 days for coring and 12 days for riser tophole casing. As riser hole casing was one of the primary objectives of the expedition, its postponement compelled a major revision of our scientific operations during the expedition. It allowed us to add coring at another planned riser site in the forearc basin (Site C0002). As a consequence, we could acquire geological and geothermal information in the shallow part of the accretionary prism and the overlying slope/forearc basin sequences at both planned riser sites (C0001 and C0002). These sites are located at vital positions and also elucidate the relationships between the growth of the accretionary prism and the evolution of the splay fault system. Coring to 458 m CSF at Site C0001 was not fully successful with regard to its intended TD of 1000 mbsf. As for Site C0002, we had to give up coring at 1057 m CSF although our intention was to core to 1400 mbsf. However, this was not because of any unexpected trouble or problem. We think that at that depth we almost reached the technical limitations of riserless coring in such a geologic setting; hence, we may have obtained possible maximum results for the accretionary prism for riserless coring. Note that Site C0002 results were additional and were not anticipated at the beginning of the expedition. Our expedition, therefore, could not fully have satisfied the original scientific objectives; however, we set up alternative targets in the course of the expedition and executed them successfully. Despite these difficulties, we believe that the overall achievement of the expedition as a "Megasplay Riser Pilot" study was satisfactory.

Operations

This section summarizes ship and drilling operations during Expedition 315. Table T1 includes hole summary data for the expedition.

Site C0001

Transit from Site C0006 to Site C0001

The *Chikyu* departed Site C0006, the last location of Expedition 314, at 1652 h on 15 November 2007. The 14 nmi transit was covered at an average speed of 3.5 kt. Rig maintenance was carried out upon arrival at Site C0001 at 2050 h on the same day.

Hole C0001E

After making up an HPCS/ESCS coring assembly with a 11-7/16 inch bit, we started running in hole at 0000 h on 17 November. A mechanical failure was found in a drawworks motor while running in hole to 1706 m drillers depth below rig floor (DRF). We pulled the assembly to the surface, and inspection of the drawworks was started at 2145 h. Trouble shooting of the drawworks A and B motors continued to 0200 h on 19 November. We made up an 11-7/16 inch HPCS/ESCS coring assembly and ran in hole to 2207 m DRF. We observed the HPCS core barrel drop through the core bit during running with core line at 1515 m DRF because of a loose connection from severe vibration induced by the strong current. The fishing operation started at 1645 h, and we successfully retrieved the core barrel at 0230 h on 20 November. We restarted running in hole to the seafloor and shot the first core at 2211.6 m DRF at 0410 h. The first core was on deck at 0500 h. HPCS coring continued until the morning of 21 November, and we cut 13 cores. Downhole temperature measurement was carried out with the APCT3 on Cores 315-C0001E-2H, 5H, 8H, and 11H. After shooting Core 315-C0001E-14H, the inner barrel could not be freed with 450 kN maximum overpull. We rotated the string under 450 kN of overpull by mistake, which resulted in a break of the inner barrel, which parted at the bottom of the second rod connection. An APCT3 tool was also lost in the hole, along with an HPCS inner barrel assembly (except for the middle/upper piston rod and landing shoulder sub). We displaced the hole with 1.3 SG kill mud and pulled out of the hole from 2335 to 2153 m DRF at 0830 h on 21 November.

Hole C0001F

After we abandoned Hole C0001E, we moved 20 m eastward and spudded Hole C0001F. After washing to 108 mbsf, we started coring with ~10 m of overlap with the previous hole. We cored 121.8 m and cut 19 cores with the HPCS. Our recovery rate was >100% for most cores; however, some of relatively deep cores showed obvious flow-in structure. Downhole temperature measurements were carried out using the APCT3 on Cores 315-C0001F-2H and 5H. Because the formation became stiff, we changed the coring system to the ESCS from the twentieth core and then cored 19.0 m and cut two cores. Core recovery was good for both cores; however, severe drilling disturbance was observed on X-ray CT scan imagery. Therefore, we decided to stop ESCS coring and switch to the RCB. We abandoned the hole by displacing with 1.3 SG kill mud and then pulled out of the hole and recovered the ROV under drifting with an average speed of 0.8 kt at 0500 h on 24 November.

Hole C0001G

We started making up a 10 ft 5/8 inch RCB assembly at 0845 h on 24 November and started running in hole from 1300 h. We spudded Hole C0001G at 0130 h on 25 November. After jetting to 74.5 mbsf, we started drilling. Just after drilling started, the ROV umbilical cable wrapped around the drill pipe. We stopped drilling and started pulling out of the hole at 0900 h. We safely recovered the ROV on board at 1500 h and confirmed it had no fatal damage.

Hole C0001H

After moving the vessel 6 nmi upcurrent with an average speed of 3.0 kt, we restarted running in hole at 1745 h on 25 November. We spudded Hole C0001H at 0330 h on 26 November, ~10 m away from the previous hole. After jetting to 74 mbsf, we started drilling with an RCB assembly with a center bit. Drilling to 230.0 m CSF, we retrieved the center bit and started RCB coring at 1445 h. The first RCB core arrived on deck at 1704 h. The ROV umbilical cable wrapped around the drill pipe at 0300 h on 27 November, but we recovered at 0530 h without retrieving it to the surface. After cutting Core 315-C0001H-20R at 412.5 m CSF, high torque to 18 kNm was observed. It reduced back to normal (3–5 kNm) after we twice pumped 10 m³ of Hi-Vis mud. Round mudstone gravel, typical of borehole caving, was observed at the top of Cores 315-C0001H-18R (~15 cm) and 20R.

Core recovery was generally as low as 30%–35% except for one core, which yielded almost full recovery. Correlation between drilling parameters and core recovery was uncertain. As weather was getting worse, we stopped coring at 448.0 m CSF after cutting Core 315-C0001H-24R and started free fall funnel installation at 1600 h on 28 November.

We completed installation of the free fall funnel by 0700 h on 29 November, and then we pulled the pipe to 35 m CSF and waited on weather for the rest of the day. As weather recovered at night, we started running in hole at 2330 h. After running the bottom-hole assembly (BHA) from 152 to 381 m CSF, we swept and reamed with Hi-Vis mud for the interval 381 to 448 m CSF. We restarted coring at 0600 h on 30 November and cut two cores from 447.2 to 457.8 m CSF. The pipe stuck while coring and was released with 350 kN overpull; we then decided to stop coring. We displaced the hole with 1.3 SG kill mud and started to pull out of the hole at 1230 h. The pipe was recovered at the surface by 2145 h. As the current was too strong to retrieve the ROV, we had to wait until the current was below the operational limit. Meanwhile, we

made up a 10-5/8 inch drilling assembly. After moving the vessel 8.6 nmi to a low-current area at 0730 h on 1 December at an average speed of 0.7 kt, we retrieved the ROV at 2045 h while drifting. We started moving the vessel 5 nmi upcurrent of the well location at 2045 h with an average speed of 3.1 kt. Meanwhile, we repaired a ROV cursor cable.

We started running in hole at 0200 h on 2 December. We launched the ROV at 0630 h and dove into the location at 0900 h. Positioning the vessel to set the bit above the free fall funnel at 1030 h, we reentered the hole at 1235 h. After washing and reaming from 299 to 458 m CSF, we started drilling at 1930 h. We reached 600 m CSF, the starting depth for coring, at 2200 h on 3 December and then repeated reaming and wiper trips several times for coring. After we spotted 57 m³ of 1.3 SG kill mud, we started pulling out of the hole at 2030 h and retrieved the BHA to the surface at 0500 h. We moved the vessel 6 nmi upcurrent and meanwhile made up an RCB coring assembly without a center bit. We started running in hole at 0900 h and launched the ROV at 1330 h. The vessel was on location at 1845 h. We reentered the hole at 2010 h and continued running in the hole to 264 m CSF. We then started washing and reaming from 268 m CSF at 2200 h. Despite repeated washing and reaming, borehole conditions did not improve. After washing and reaming to 449 m CSF, we finally decided to abandon the hole at 1300 h on 5 December. We displaced the hole with 50 m³ of 1.3 SG kill mud and picked up the coring assembly to the seafloor. We moved the vessel 60 m eastward and spudded a new hole (C0001I).

Hole C0001I

We dropped a center bit and then spudded the new hole at 1600 h on 5 December. After jetting to 70 mbsf, we started drilling at 1700 h with a 10-5/8 inch RCB assembly with a center bit. Drilling to 425 m CSF was relatively smooth. At every pipe stand, 10 m³ of Hi-Vis mud was spotted. On 6 December, while picking up from 458 to 340 m BSF to change the wash pipe, both upper and lower Inline Blow-Out Preventors (IBOPs; back valves at the top drive) were repaired. Running in hole started at 1400 h. We started drilling from 458 m CSF at 1630 h. After drilling to 520 m CSF, we repeated washing and reaming to 520 m CSF. While backreaming from 434 to 464 m CSF, we had a pipe stick at 464 m CSF. We managed to free the pipe with 700 kN of overpull. After escaping from this zone, we gave up further drilling and coring at 0315 h on 7 December. After displacing the hole with 35 m³ of 1.5 SG kill mud, we started pulling out of the hole at 0900 h and finished at 1400 h. The ROV dove to retrieve transponders at 1600 h. Meanwhile, we changed the saver sub and repaired a leak on

the top drive system. Four transponders were recovered at 0230 h on 8 December. We left the location for Site C0002 at 0230 h.

Site C0002

Transit from Site C0001 to C0002

The *Chikyu* departed Site C0001 at 0230 h on 8 December 2007. The 7 nmi transit was covered at an average speed of 2.8 kt. We arrived at Site C0002 at 0530 h on the same day.

Hole C0002B

The vessel was on location at 0530 h on 8 December. Deployment and calibration of four transponders occurred from 0530 h to 1930 h. The vessel moved 4 nmi upcurrent from 1930 to 2215 h at an average speed of 1.6 kt. We started making up and running a 10-5/8 inch RCB assembly at 2215 h. In the meantime, minor troubleshooting of the dynamic positioning system was carried out. We spudded the hole at 0600 h on 9 December. After jetting to 50 mbsf, we started drilling with an RCB coring assembly with a center bit at 0745 h. While drilling to 181 m CSF, a problem with the top drive was discovered at 1300 h. We checked it and made repairs to the changing bolt until 1815 h. We started running in hole at 1815 h, and we restarted drilling from 181 m CSF at 1830 h. We reached the starting coring depth (475 m CSF) at 0215 h on 10 December and installed a sinker bar. We retrieved the center bit and then dropped an inner barrel and started coring at 0530 h. We continued coring until 0700 h on 11 December and cut 22 cores in the interval from 475 to 675 m CSF. As leaking was found on the Crown-Mounted Heave Compensator (CMC) booster line at 0700 h, we spotted 10 m³ of Hi-Vis mud and retrieved an inner barrel and a sinker bar. Repairs were completed by 1530 h. After washing and reaming from 634 to 669 m CSF, we installed a sinker bar and restarted coring at 1730 h. After cutting Core 315-C0002B-23R, we could not recover the inner barrel. A swivel assembly shaft of the inner barrel was left down the hole. We ran a fishing tool (core catcher) in the hole with the coring line and were able to retrieve the assembly at 2230 h. We restarted coring at 2315 h on 11 December and cut 39 cores by 1645 h on 13 December. The drill pipe stuck twice, once at 1029 m CSF at 1650 h and another time at 1030 m CSF at 1715 h on 14 December, but came free with 300 kN of overpull each time. After cutting four more cores, hole conditions became worse below 1057 m CSF at 2230 h. The drill pipe was packed off and was freed by 300 kN of overpull. We washed and reamed the hole repeatedly with sweeping Hi-Vis mud until the next morning; however, hole condi-

tions did not become better. We finally decided to stop RCB coring and abandon the hole at 1345 h on 15 December. We displaced the hole with 1.3 SG kill mud and pulled out of the hole until 2100 h. The ROV was recovered at 1835 h. We moved the vessel 6 nmi upcurrent at 2100 h on 15 December, at an average speed of 1.5 kt.

Hole C0002C

The vessel was on location at 0130 h on 16 December. We made up an 11-7/16 inch HPCS assembly at 0630 h and started running in hole at 0830 h. We installed a sinker bar and an inner barrel at 1530 h and cut two HPCS cores until 1815 h. We moved the vessel 10 m away from the hole for the next hole coring.

Hole C0002D

The vessel was on location at 1830 h on 16 December, and we continued HPCS coring at 1830 h. We cut 13 cores with the HPCS until 0830 h on 17 December. With 450 kN of overpull on Core 315-C0002D-13H at 120 m CSF, we overdrilled from 110 to 113 m CSF. We pulled the core line winch to the surface and found that we had not recovered the inner barrel (the sinker bar pin was sheared). We installed a new latch head and ran back in and latched. After another 2 m of overdrill, we attempted to pull free and released the inner barrel with 400 kN of overpull. We changed the latch head and replaced shear pins and V-packings on the inner barrel. We continued HPCS coring from 114 to 120 m CSF. We had high overpull (450 kN) again and overdrilled 5 m; the barrel came free with 400 kN of overpull. After recovering this core, we dropped the ESCS BHA for drilling. Having verified its landing, we started drilling at 1600 h from 129 m CSF. We ran a sinker bar assembly in the hole and recovered the ESCS. We then ran the APCT3 in the hole and performed HPCS coring at 150 m CSF. To free the barrel, 200 kN of overpull was needed. We recovered the HPCS core and dropped the ESCS again. We verified its landing and then started drilling from 159 m CSF at 2015 h. We ran the sinker bar assembly in the hole and recovered the ESCS at 2300 h. The final HPCS core was taken from 200 m CSF at 0110 h on 18 December. A total of 18 cores were cut in this hole. Downhole temperature measurement by the APCT3 was attempted on Cores 315-C0002D-2H, 4H, 6H, 8H, 10H, 12H, 16H, and 18H; six of these were successful. We displaced the hole with 26 m^3 of 1.3 SG kill mud and pulled out of the hole to the surface from 0215 h to 0545 h. We moved the vessel and then launched the ROV at 0730 h and retrieved four transponders by 1345 h. The vessel left for Expedition 316 Site C0004 at 1345 h on 18 December.

References

Ando, M., 1975. Source mechanisms and tectonic significance of historical earthquakes along the Nankai Trough, Japan. *Tectonophysics,* 27(2):119–140. **doi:10.1016/0040-1951(75)90102-X**

Ashi, J., Kuramoto, S., Morita, S., Tsunogai, U., Goto, S., Kojima, S., Okamoto, T., Ishimura, T., Ijiri, A., Toki, T., Kudo, S., Asai, S., and Utsumi, M., 2002. Structure and cold seep of the Nankai accretionary prism off Kumano—outline of the off Kumano survey during YK01-04 Leg 2 cruise. *JAMSTEC J. Deep Sea Res.,* 20:1–8.

Ashi, J., Lallemant, S., and Masago, H., 2007. NanTroSEIZE Stage 1: NanTroSEIZE megasplay riser pilot. *IODP Sci. Prosp.,* 315. **doi:10.2204/iodp.sp.315.2007**

Baba, T., and Cummins, P.R., 2005. Contiguous rupture areas of two Nankai Trough earthquakes revealed by high-resolution tsunami waveform inversion. *Geophys. Res. Lett.,* 32(8):L08305. **doi:10.1029/2004GL022320**

Berner, R.A., 1980. *Early Diagenesis: A Theoretical Approach:* Princeton, NJ (Princeton Univ. Press).

Cowan, D.S., 1982. Origin of "vein structure" in slope sediments on the inner slope of the Middle America Trench off Guatemala. *In* Aubouin, J., von Huene, R., et al., *Init. Repts. DSDP,* 67: Washington, DC (U.S. Govt. Printing Office), 645–650. **doi:10.2973/dsdp.proc.67.132.1982**

Emmermann, R., and Lauterjung, J., 1997. The German Continental Deep Drilling Program KTB: overview and major results. *J. Geophys. Res.,* 102(B8):18179–18202. **doi:10.1029/96JB03945**

Goto, S., Kuramoto, S., Ashi, J., and Yamano, M., 2003. Heat and fluid fluxes at a biological community site on the Nankai accretionary prism off Kii Peninsula. In *IUGG Gen. Assembly—State of the Planet: Frontiers and Challenges,* 23:A198.

Gradstein, F.M., Ogg, J.G., and Smith, A. (Eds.), 2004. *A Geologic Time Scale 2004:* Cambridge (Cambridge Univ. Press). **http://www.stratigraphy.org/**

Hori, T., Kato, N., Hirahara, K., Baba, T., and Kaneda, Y., 2004. A numerical simulation of earthquake cycles along the Nankai Trough in southwest Japan: lateral variation in frictional property due to the slab geometry controls the nucleation position. *Earth Planet. Sci. Lett.,* 228(3–4):215–226. **doi:10.1016/j.epsl.2004.09.033**

Huchon, P., Tokuyama, H., Lallemant, S.J., Taira, A., Henry, P., Mazzotti, S., and Le Pichon, X., 1998. Pervasive dextral strike-slip faulting within the backstop of the eastern Nankai wedge confirmed by deep-towed seismic data (*KAIKO-TOKAI* '96 cruise). *C. R. Acad. I., Ser. IIa: Sci. Terre Planetes,* 326(12):869–875.

Ichinose, G.A., Thio, H.K., Somerville, P.G., Sato, T., and Ishii, T., 2003. Rupture process of the 1944 Tonankai earthquake (M_s 8.1) from the inversion of teleseismic and regional seismograms. *J. Geophys. Res.,* 108(B10):2497. **doi:10.1029/2003JB002393**

Kame, N., Rice, J.R., and Dmowska, R., 2003. Effects of prestress state and rupture velocity on dynamic fault branching. *J. Geophys. Res.,* 108(B5):2265. **doi:10.1029/2002JB002189**

Kikuchi, M., Nakamura, M., and Yoshikawa, K., 2003. Source rupture processes of the 1944 Tonankai earthquake and the 1945 Mikawa earthquake derived from low-gain seismograms. *Earth, Planet. Space,* 55(4):159–172.

Kinoshita, M., Goto, S., Hamamoto, H., and Yamano, M., 2003. Heat flow distribution and thermal regime across the Nankai accretionary complex. *Eos, Trans. Am. Geophys. Union,* 84(46)(Suppl.):T42C-06 (Abstract).

Kinoshita, M., Tobin, H., Moe, K.T., and the Expedition 314 Scientists, 2008. NanTroSEIZE Stage 1: NanTroSEIZE LWD transect. *IODP Prel. Rept.,* 314. **doi:10.2204/iodp.pr.314.2008**

Kuramoto, S., Ashi, J., Greinert, J., Gulick, S., Ishimura, T., Morita, S., Nakamura, K., Okada, M., Okamoto, T., Rickert, D., Saito, S., Suess, E., Tsunogai, U., and Tomosugi, T., 2001. Surface observations of subduction-related mud volcanoes and larger thrust sheets in the Nankai subduction margin: report on YK00-10 and YK01-04 cruises. *JAMSTEC J. Deep Sea Res.,* 19:131–139.

Miyazaki, S., and Heki, K., 2001. Crustal velocity field of southwest Japan: subduction and arc-arc collision. *J. Geophys. Res.,* 106(B3):4305–4326. **doi:10.1029/2000JB900312**

Moore, G.F., Bangs, N.L., Taira, A., Kuramoto, S., Pangborn, E., and Tobin, H.J., 2007. Three-dimensional splay fault geometry and implications for tsunami generation. *Science,* 318(5853):1128–1131. **doi:10.1126/science.1147195**

Moore, G.F., Taira, A., Klaus, A., Becker, L., Boeckel, B., Cragg, B.A., Dean, A., Fergusson, C.L., Henry, P., Hirano, S., Hisamitsu, T., Hunze, S., Kastner, M., Maltman, A.J., Morgan, J.K., Murakami, Y., Saffer, D.M., Sánchez-Gómez, M., Screaton, E.J., Smith, D.C., Spivack, A.J., Steurer, J., Tobin, H.J., Ujiie, K., Underwood, M.B., and Wilson, M., 2001. New insights into deformation and fluid flow processes in the Nankai Trough accretionary prism: results of Ocean Drilling Program Leg 190. *Geochem., Geophys., Geosyst.,* 2(10). **doi:10.1029/2001GC000166**

Nakanishi, A., Takahashi, N., Park, J.-O., Miura, S., Kodaira, S., Kaneda, Y., Hirata, N., Iwasaki, T., and Nakamura, M., 2002. Crustal structure across the coseismic rupture zone of the 1944 Tonankai earthquake, the central Nankai Trough seismogenic zone. *J. Geophys. Res.,* 107(B1):2007. **doi:10.1029/2001JB000424**

Obana, K., Kodaira, S., and Kaneda, Y., 2004. Microseismicity around rupture area of the 1944 Tonankai earthquake from ocean bottom seismograph observations. *Earth Planet. Sci. Lett.,* 222(2):561–572. **doi:10.1016/j.epsl.2004.02.032**

Obara, K., and Ito, Y., 2005. Very low frequency earthquakes excited by the 2004 off the Kii Peninsula earthquakes: a dynamic deformation process in the large accretionary prism. *Earth, Planet. Space,* 57(4):321–326.

Ogawa, Y., 1980. Beard-like veinlet structure as fracture cleavage in the Neogene siltstone in the Miura and Boso Peninsulas, central Japan. *Sci. Rep. Dept. Geol., Kyushu Univ.,* 13:321–327.

Park, J.-O., Tsuru, T., Kodaira, S., Cummins, P.R., and Kaneda, Y., 2002. Splay fault branching along the Nankai subduction zone. *Science,* 297(5584):1157–1160. **doi:10.1126/science.1074111**

Seno, T., Stein, S., and Gripp, A.E., 1993. A model for the motion of the Philippine Sea plate consistent with NUVEL-1 and geological data. *J. Geophys. Res.,* 98:17941–17948.

Tanioka, Y., and Satake, K., 2001. Detailed coseismic slip distribution of the 1944 Tonankai earthquake estimated from tsunami waveforms. *Geophys. Res. Lett.,* 28(6):1075–1078. **doi:10.1029/2000GL012284**

Toki, T., Tsunogai, U., Gamo, T., Kuramoto, S., and Ashi, J., 2004. Detection of low-chloride fluids beneath a cold seep field on the Nankai accretionary wedge off Kumano, south of Japan. *Earth Plant. Sci. Lett.,* 228(1–2):37–47. **doi:10.1016/j.epsl.2004.09.007**

Wang, K., and Hu, Y., 2006. Accretionary prisms in subduction earthquake cycles: the theory of dynamic Coulomb wedge. *J. Geophys. Res.,* 111(B6):B06410. **doi:10.1029/2005JB004094**

Table T1. Hole Summary, Expedition 315.

Hole	Location	Water depth (mbsl)	Number of cores	Drilled depth (m)	Interval cored (m)	Recovered (m)	Recovery (%)	Comments
C0001E	33°14.3442'N, 136°42.6924'E	2198.0	13 HPCS	118.10	118.10	112.67	95.4	Lost inner core barrel in hole
C0001F	33°14.3437'N, 136°42.7067'E	2197.0	19 HPCS, 2 ESCS	248.83	140.80	137.50	97.7	
C0001G	33°14.3237'N, 136°42.6933'E	2196.5	NA	74.50	NA	NA	NA	ROV cable tangled around drill pipe
C0001H	33°14.3233'N, 136°42.6840'E	2197.0	26 RCB	590.50	228.60	126.30	55.2	Hole caving
C0001I	33°14.2030'N, 136°42.4330'E	2198.5	NA	520.00	NA	NA	NA	Hole caving
	Site C0001 totals:		32 HPCS, 2 ESCS, 26 RCB	1551.93	487.50	376.47	77.2	
C0002B	33°17.9928'N, 136°38.2029'E	1937.5	66 RCB	1057.00	582.00	208.30	35.8	
C0002C	33°18.0026'N, 136°38.1869'E	1936.6	2 HPCS	13.77	13.80	13.77	99.8	
C0002D	33°18.0075'N, 136°38.1910'E	1937.1	16 HPCS, 2 ESCS	204.00	204.00	161.90	79.4	
	Site C0002 totals:		18 HPCS, 2 ESCS, 66 RCB	1274.77	799.80	383.97	48.0	

Note: HPCS = hydraulic piston coring system, ESCS = extended shoe coring system, NA = no core recovered, RCB = rotary core barrel, ROV = remotely operated vehicle.

Figure F1. Map of Kumano Basin region with proposed Stage 1 drill sites. Red dots = primary sites, green dots = alternate sites, black outline = 3-D seismic volume region.
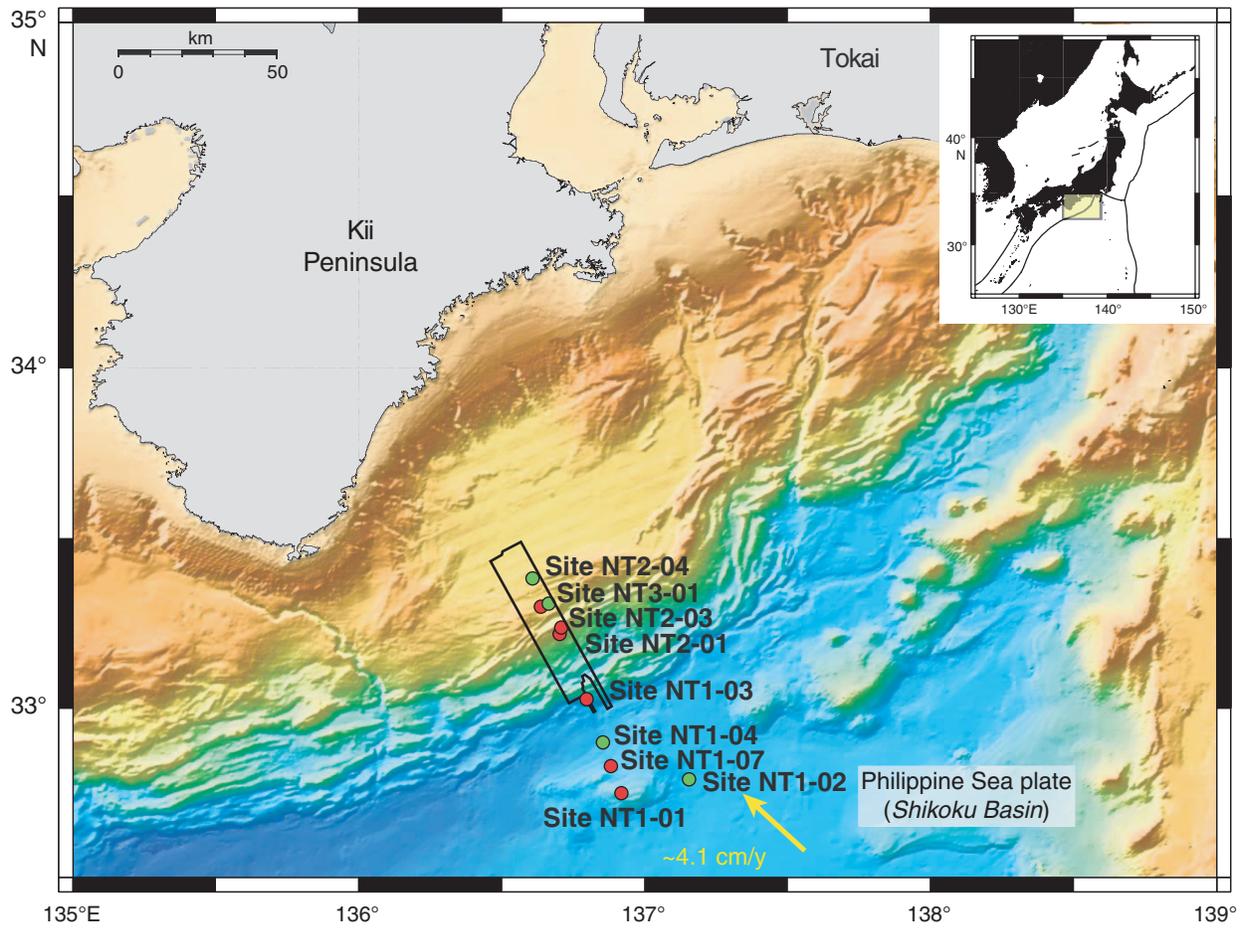
Figure F2. Location of Sites C0001 and C0002. Other sites drilled during Expedition 314 (Sites C0003, C0004, and C0006) are also shown. Box = area in Figure **F3.**
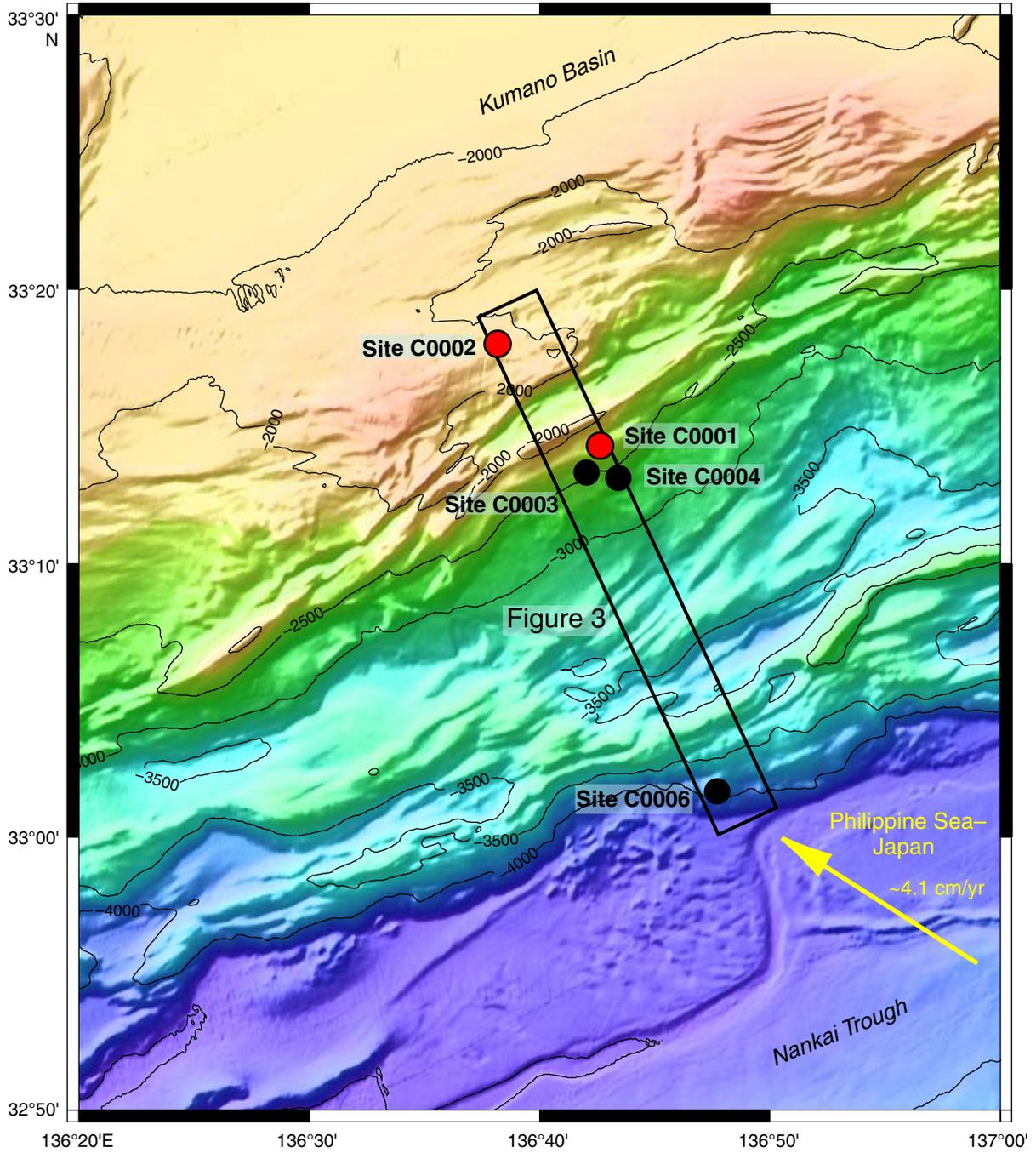
Figure F3. Regional seismic image across the main Stage 1 sites based on 3-D seismic volume (Moore et al., 2007). Note the two in-line profiles (IL 2675 and IL 2435) are spliced near the toe of the accretionary prism. Sites C0002 and C0003 are located on different inlines. BSR = bottom-simulating reflector, VE = vertical exaggeration.
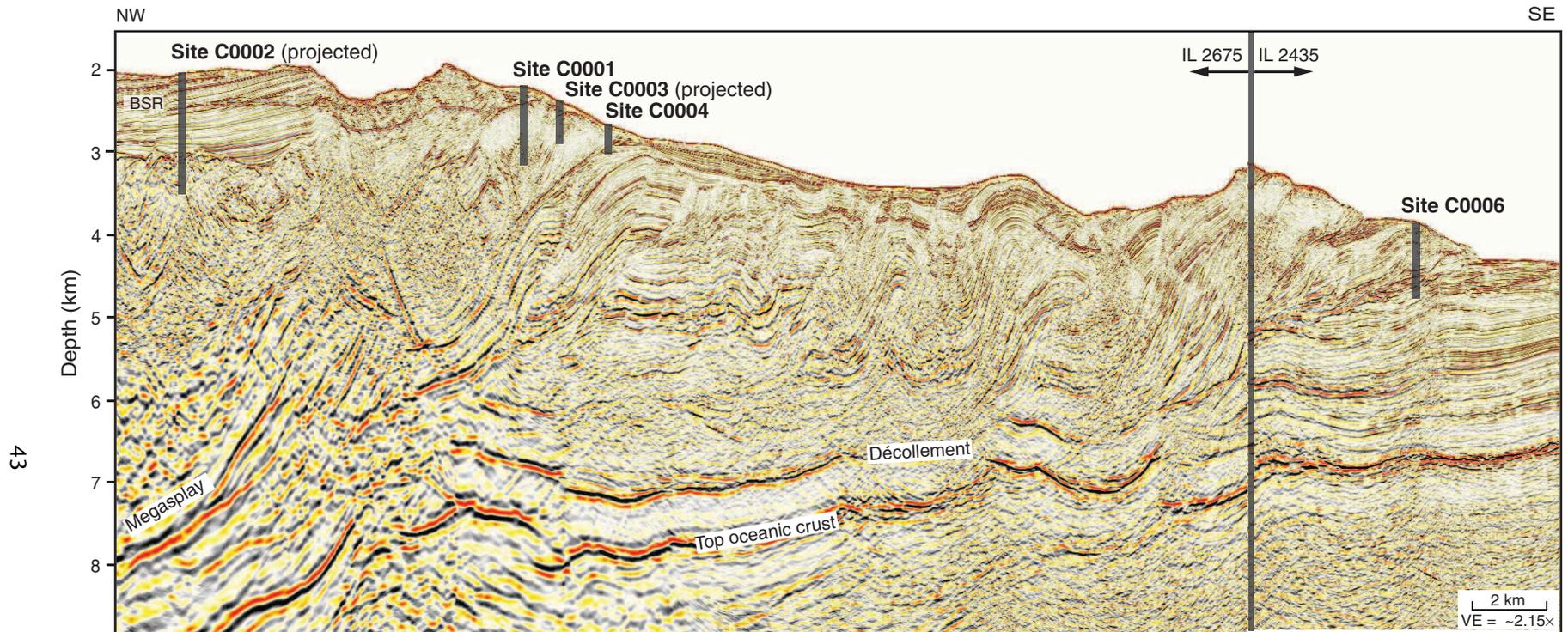
Figure F4. Drilling strategies for **(A)** Site C0001 and **(B)** Site C0002. HPCS = hydraulic piston coring system, ESCS = extended shoe coring system, RCB = rotary core barrel.
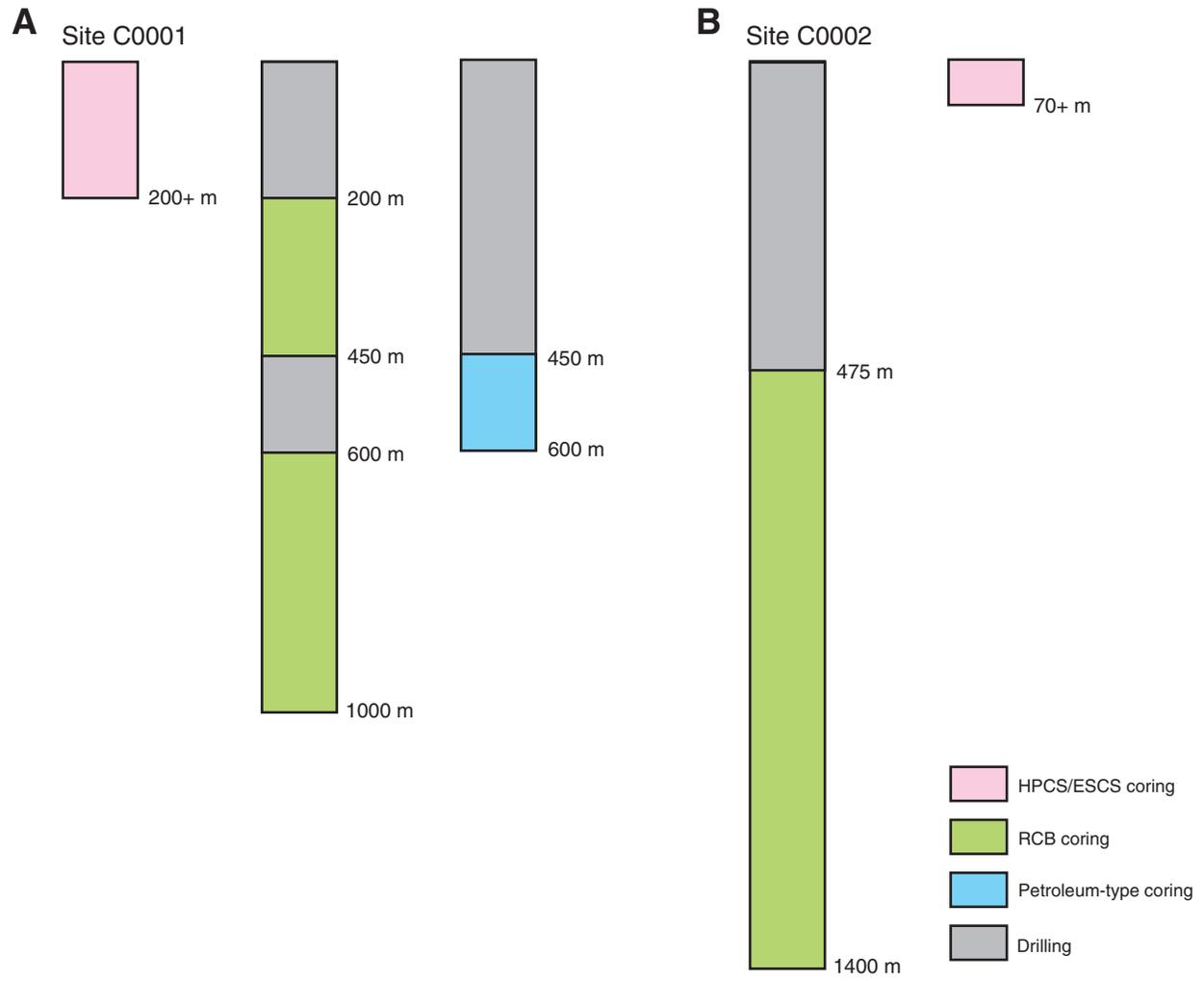
Figure F5. Stratigraphic summary, Site C0001. CSF = core depth below seafloor.
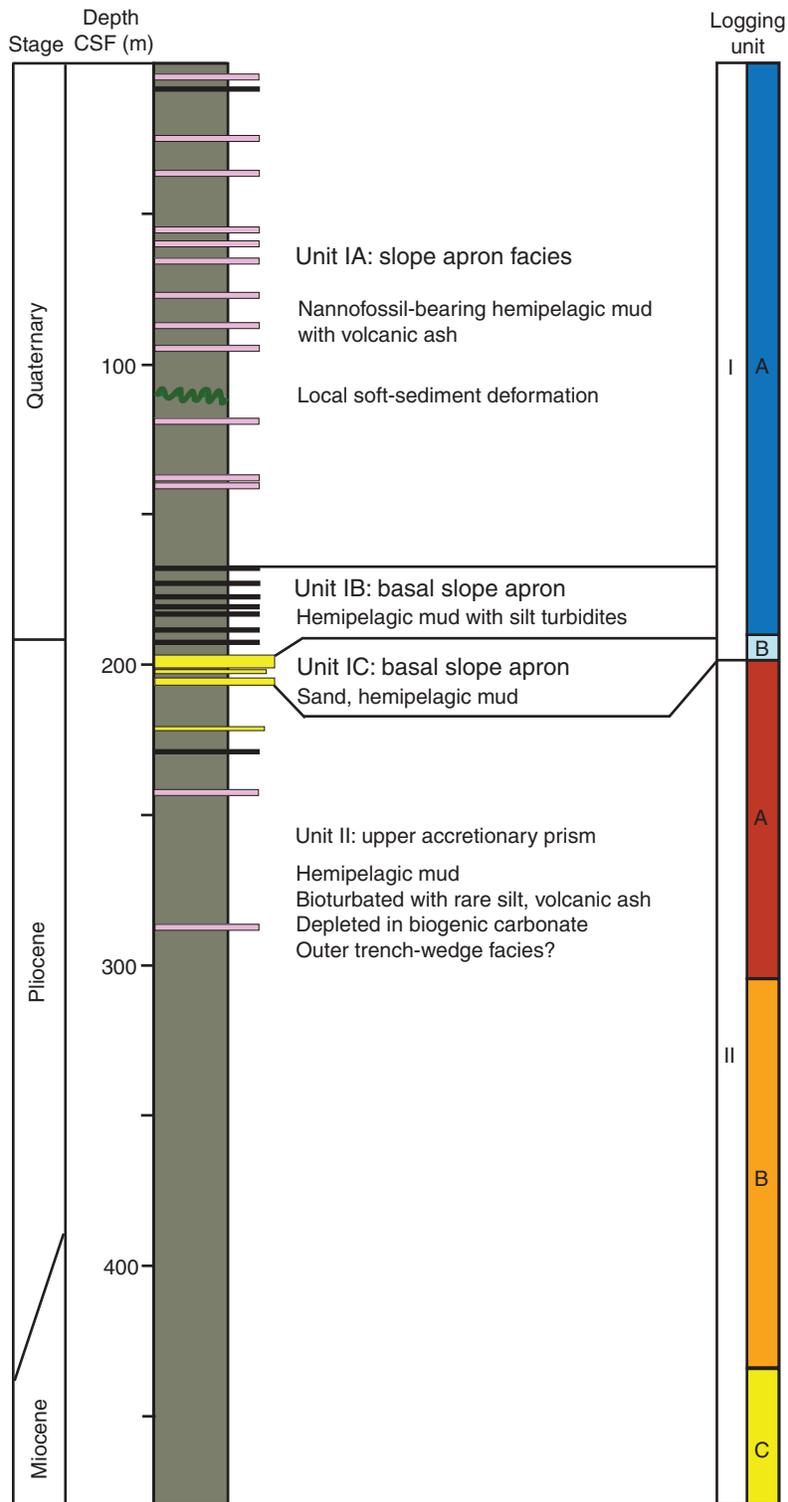
Figure F6. Remnant inclination after 20 mT AF demagnetization in the interval between 0 and 230 m CSF. The magnetic polarity interpretation (black = normal polarity, white = reversed polarity) is displayed on the right. CSF = core depth below seafloor.
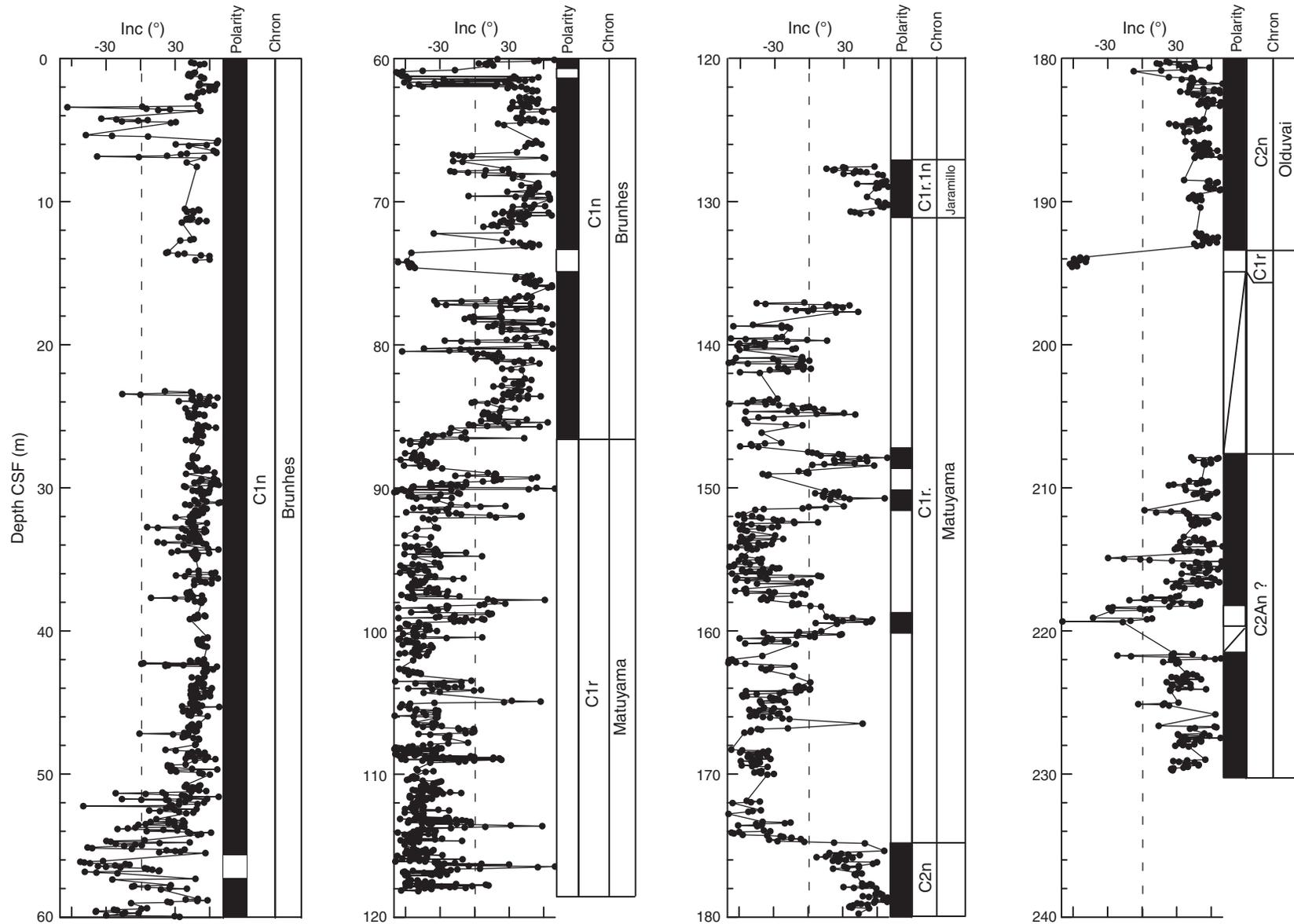
Figure F7. A. Synthetic stratigraphic log. **B, C.** Frequency of shear zones and faults in cores. **D, E.** Dip and dip direction of beddings. **F–I.** Dip of shear zones, normal faults, thrusts, and strike-slip faults. CSF = core depth below seafloor.
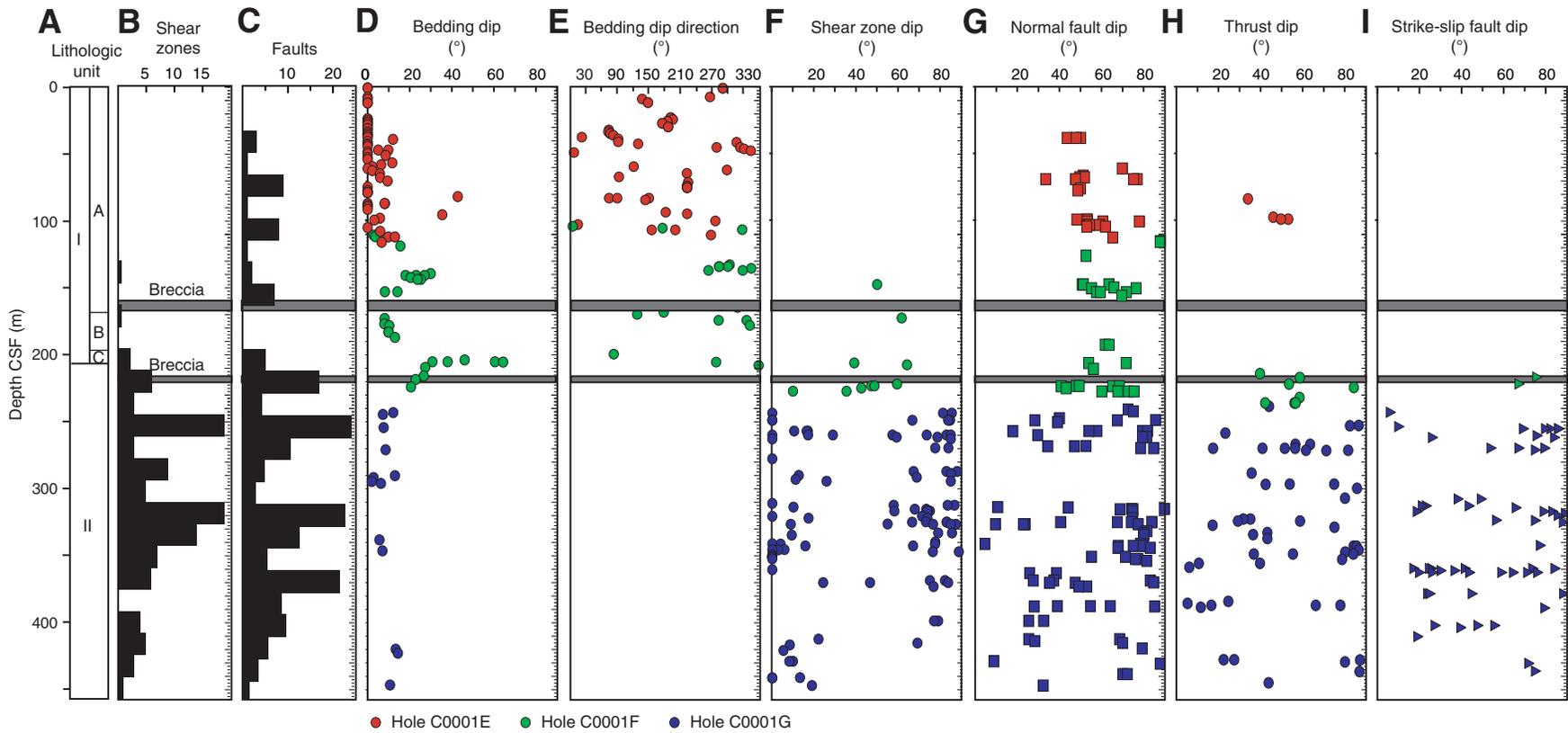
Figure F8. Concentrations of sulfate, alkalinity, phosphate and ammonium, salinity, chlorine, and major cations (Na, K, Ca, and Mg) in interstitial waters from Site C0001. Salinity is calculated as total dissolved solutes. CSF = core depth below seafloor.
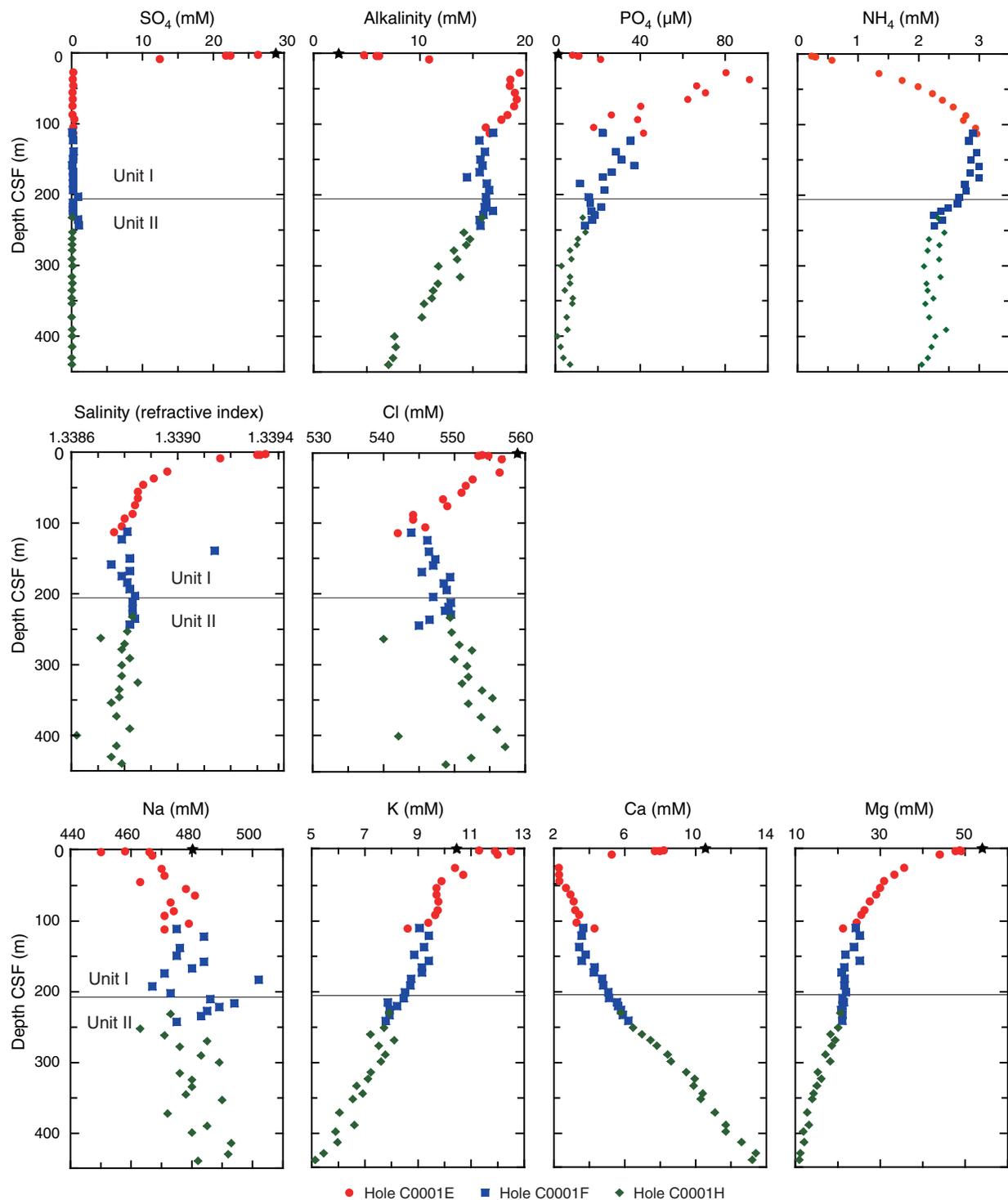
Figure F9. Depth profiles of methane, ethane, and propane concentrations in headspace samples from Site C0001. Concentrations of calcium carbonate ($CaCO_3$), total organic carbon (TOC), carbon to nitrogen (C/N) ratio, and total sulfur (TS) with depth from sediment samples. CSF = core depth below seafloor.
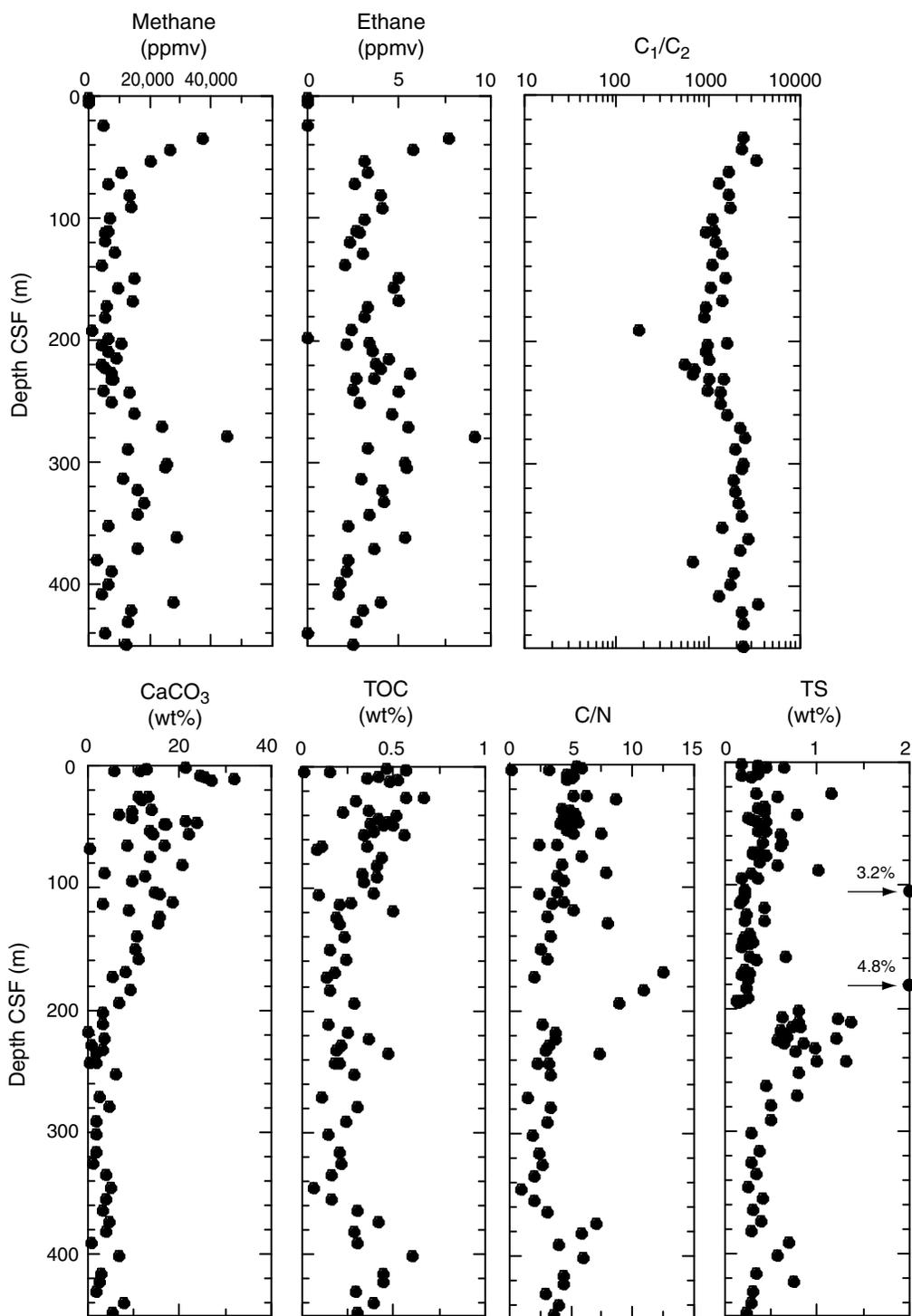
Figure F10. Measurements vs. depth at Site C0001. **A.** MAD porosity. **B.** MAD bulk density. **C.** MAD grain density. **D.** Shear strength. **E.** Thermal conductivity. CSF = core depth below seafloor.
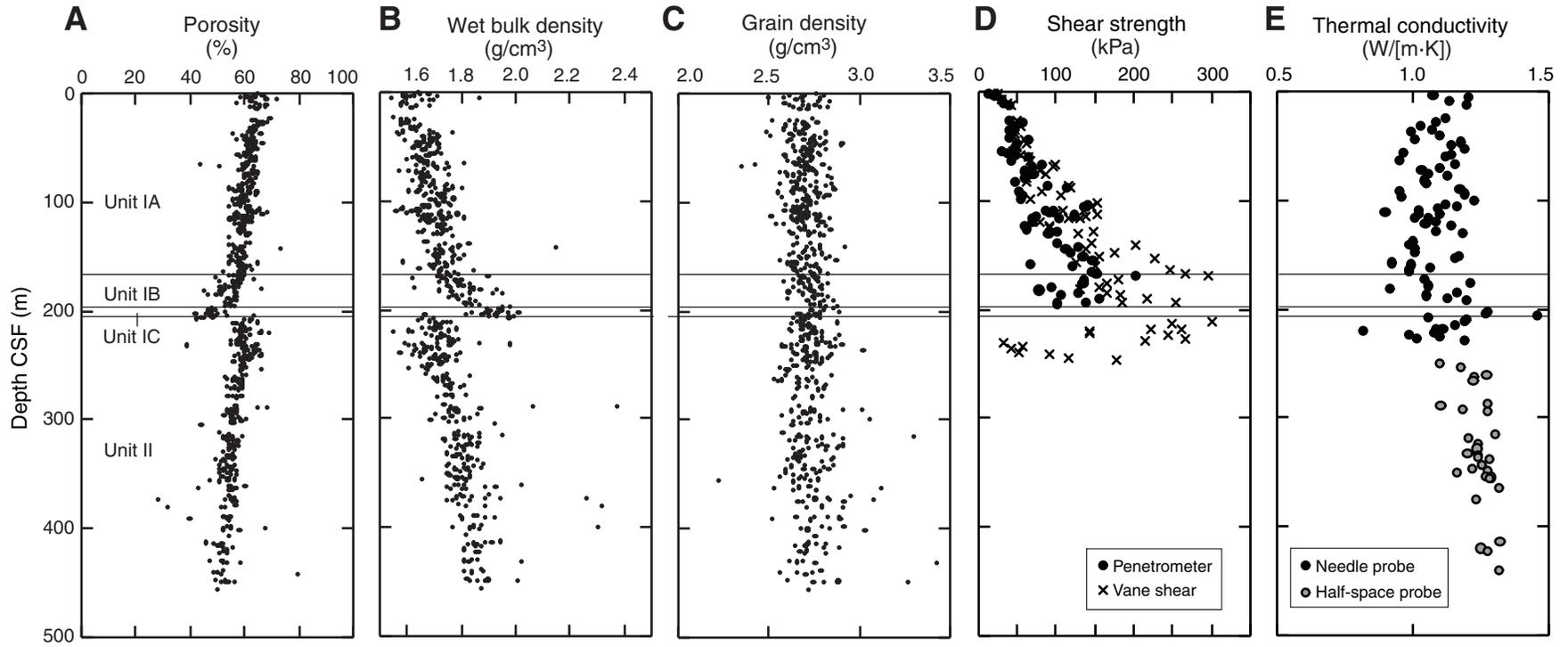
Figure F11. Stratigraphic summary, Hole C0002B. CSF = core depth below seafloor.
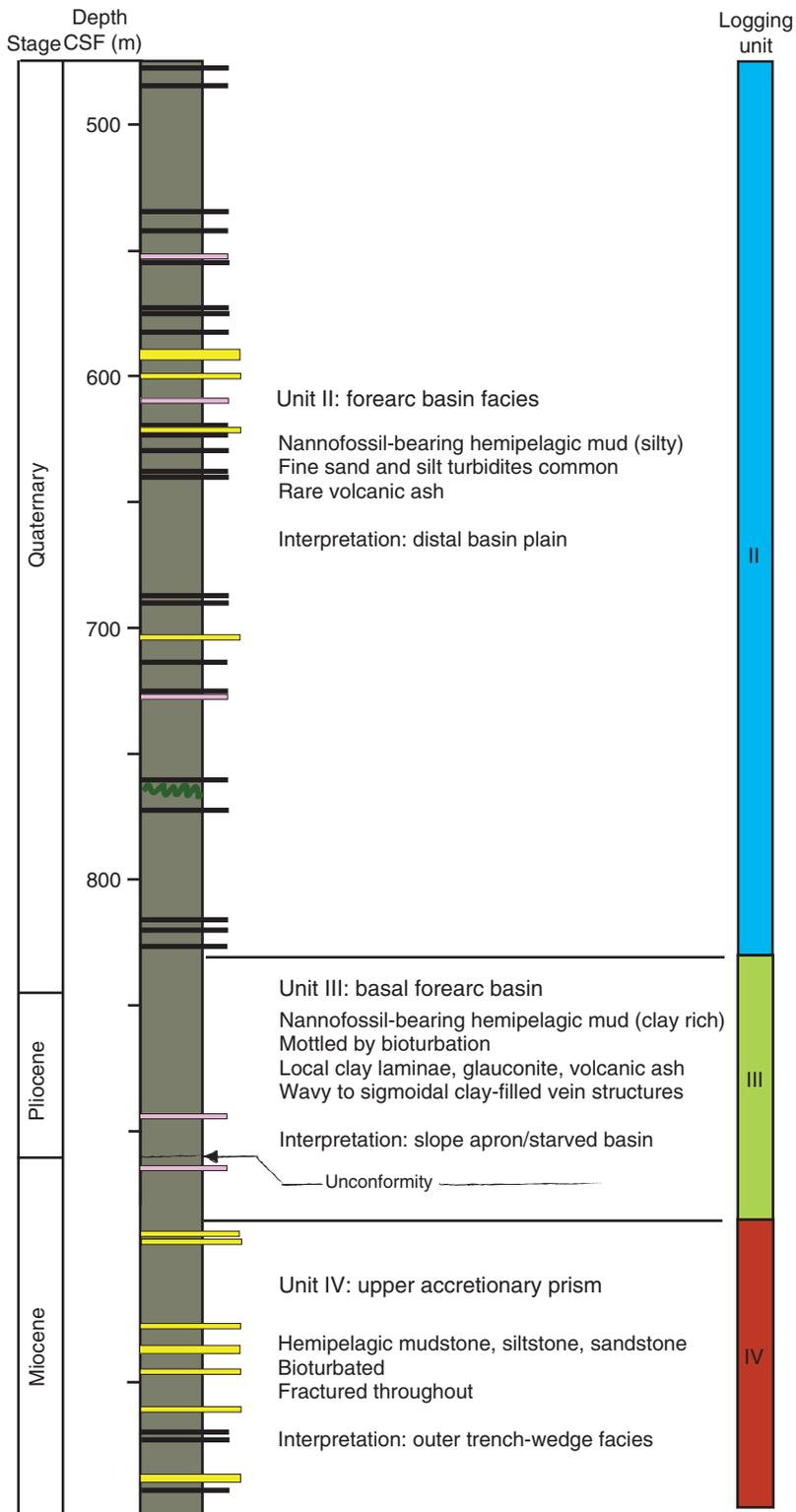
Figure F12. Measurements vs. depth in Hole C0002B. **A**, **B.** Dip angle of bedding, fissility, faults, and shear zones. **C.** Magnetic inclination plots. Broken lines indicate the expected inclinations calculated from the latitude of location. CSF = core depth below seafloor.
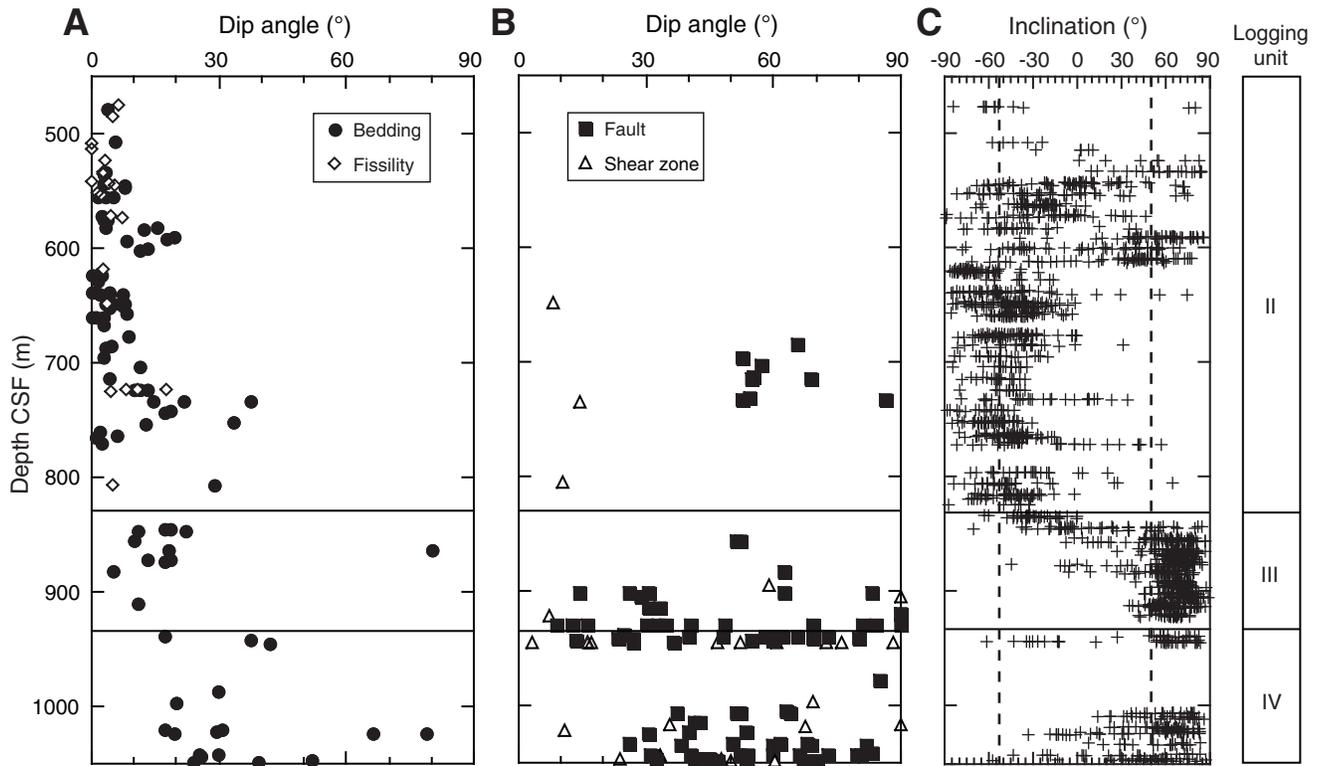
Figure F13. Concentrations of sulfate, alkalinity, phosphate, ammonium, salinity, chlorine, and major cations (Na, K, Ca, and Mg) in interstitial waters from Hole C0002B. CSF = core depth below seafloor.
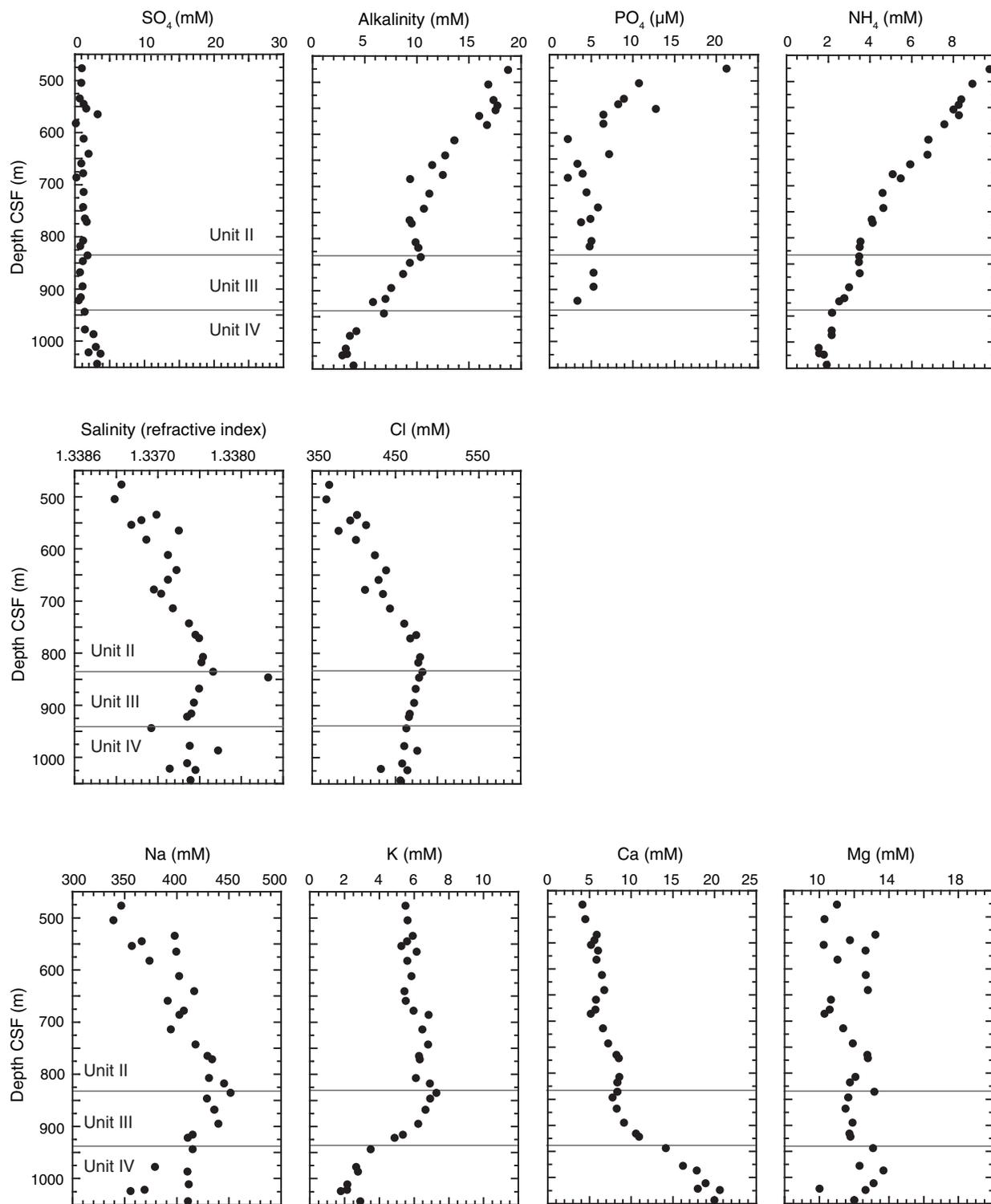
Figure F14. Depth profiles of methane along with ethane and propane concentrations in headspace samples from Hole C0002B. Concentrations of calcium carbonate ($CaCO_3$), total organic carbon (TOC), carbon to nitrogen (C/N) ratio, and total sulfur (TS) with depth from sediment samples. CSF = core depth below seafloor.
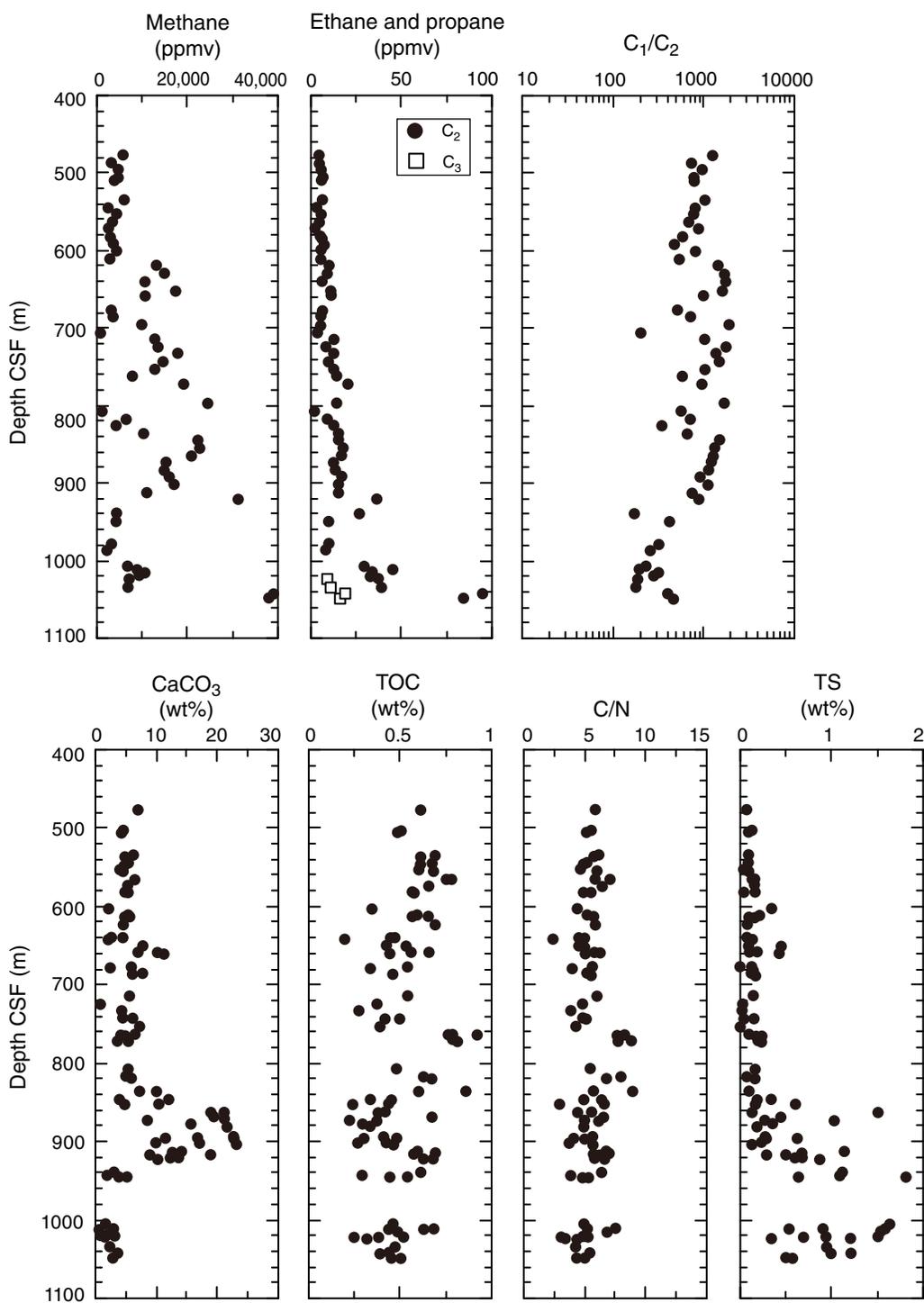
Figure F15. Measurements vs. depth at Hole C0002B. **A.** MAD porosity. **B.** MAD density. **C.** MAD grain density. **D.** Thermal conductivity. CSF = core depth below seafloor.